

## Supporting information

# Nuclear Spin Hyperpolarization with *ansa*- Aminoboranes: A Metal-Free Perspective for Parahydrogen-Induced Polarization

Vladimir V. Zhivonitko,<sup>\*,†,‡</sup> Kristina Sorochkina,<sup>¶</sup> Konstantin Chernichenko,<sup>¶</sup> Bianka Kótai,<sup>‡</sup>  
Tamás Földes,<sup>‡</sup> Imre Pápai,<sup>‡</sup> Ville-Veikko Telkki,<sup>+</sup> Timo Repo<sup>¶</sup> and Igor Koptyug<sup>†,‡</sup>

<sup>†</sup>Laboratory of Magnetic Resonance Microimaging, International Tomography Center SB RAS,  
Institutskaya St. 3A, 630090 Novosibirsk, Russia. E-mail: [v\\_zhivonitko@tomo.nsc.ru](mailto:v_zhivonitko@tomo.nsc.ru)

<sup>‡</sup>Department of Natural Sciences, Novosibirsk State University, Pirogova St. 2, 630090  
Novosibirsk, Russia.

<sup>¶</sup>Department of Chemistry, Laboratory of Inorganic Chemistry, University of Helsinki, A. I.  
Virtasen aukio 1, 00014 Helsinki, Finland.

<sup>‡</sup>Research Centre for Natural Sciences, Hungarian Academy of Sciences, Magyar Tudósok  
Körútja 2, H-1117 Budapest, Hungary.

<sup>+</sup>NMR Research Unit, University of Oulu, P.O.Box 3000, 90014 Oulu, Finland.

## -CONTENTS-

1	Full sets of variable temperature $^1\text{H}$ NMR spectra of AABs and para- $\text{H}_2$ .....	4
2	Kinetic and thermodynamic parameter determination .....	8
3	Actual values of PHIP signal attenuation factors calculated for the dimensionless parameters listed in Table 2 of the main text for the AABs under study .....	11
4	Numerical simulations of $^1\text{H}$ NMR spectra with presence of chemical exchange .....	13
5	Derivation of analytical formula for $I_z I_z$ amplitude accommodated in AAB- $\text{H}_2$ molecules under reversible chemical exchange conditions and para- $\text{H}_2$ bubbling .....	15
6	Preparation of <i>ansa</i> -aminoboranes .....	17
6.1	1-(2-(Diphenylboryl)phenyl)-2,2,6,6-tetramethylpiperidine (PhenylCAT).....	17
6.2	Hydrogen addition to PhenylCAT.....	20
6.3	1-(2-(Dimesitylboryl)phenyl)-2,2,6,6-tetramethylpiperidine (MesitylCAT).....	22
6.4	Hydrogen addition to MesitylCAT .....	25
6.5	1-(2-(Bis(2-isopropylphenyl)methyl)phenyl)-2,2,6,6-tetramethylpiperidine (iPrPhenylCAT) .....	28
6.6	Hydrogen addition to iPrPhenylCAT.....	32
7	Computational results .....	35
7.1	Cartesian coordinates of BorylCAT- $\text{H}_2$ and the $\text{BH}_3$ rotation TS.....	37
8	REFERENCES .....	39

## -FIGURES AND TABLES-

<b>Figure S1.</b> $^{14}\text{N}$ -decoupled $^1\text{H}$ NMR spectra acquired after para- $\text{H}_2$ bubbling through BorylCAT solution in methylene chloride- $\text{d}_2$ . The acquisition temperatures are shown in the figure.....	4
<b>Figure S2.</b> $^{14}\text{N}$ -decoupled $^1\text{H}$ NMR spectra acquired after para- $\text{H}_2$ bubbling through PhenylCAT solution in methylene chloride- $\text{d}_2$ . The acquisition temperatures are shown in the figure.....	5
<b>Figure S3.</b> $^{14}\text{N}$ -decoupled $^1\text{H}$ NMR spectra acquired after para- $\text{H}_2$ bubbling through iPrPhenylCAT solution in methylene chloride- $\text{d}_2$ . The acquisition temperatures are shown in the figure. ....	6
<b>Figure S4.</b> $^{14}\text{N}$ -decoupled $^1\text{H}$ NMR spectra acquired after para- $\text{H}_2$ bubbling through MesitylCAT solution in methylene chloride- $\text{d}_2$ . The acquisition temperatures are shown in the figure.....	7
<b>Figure S5.</b> Eyring plot for BorylCAT compound. Experimental points are shown with circles and the linear fitting result is shown with magenta line. The parameters obtained from the fitting are shown in the title along with accuracy bounds of 95% probability. ....	8
<b>Figure S6.</b> Eyring plot for PhenylCAT compound. Experimental points are shown with circles and the linear fitting result is shown with magenta line. The parameters obtained from the fitting are shown in the title along with accuracy bounds of 95% probability. ....	9

<b>Figure S7.</b> Eyring plot for iPrPhenylCAT compound. Experimental points are shown with circles and the linear fitting result is shown with magenta line. The parameters obtained from the fitting are shown in the title along with accuracy bounds of 95% probability. ....	10
<b>Figure S8.</b> Eyring plot for MesitylCAT compound. Experimental points are shown with circles and the linear fitting result is shown with magenta line. The parameters obtained from the fitting are shown in the title along with accuracy bounds of 95% probability. ....	11
<b>Table S1.</b> PHIP signal attenuation factors calculated using characteristic dimensionless parameters from Table 2 (main text) for the AABs under study. ....	12
<b>Figure S9.</b> Simulation results of $^1\text{H}$ NMR spectra for $\text{AX}_3$ spin system (a model for BorylCAT- $\text{H}_2$ ), in which a pair of AX protons exchanges chemically with $\text{B}_2$ spin system (a model for molecular $\text{H}_2$ ). The simulation includes numerical propagation of the density operator under the action of coherent nuclear spin Hamiltonian superoperator as well as kinetic and uncorrelated relaxation Liouvillian operators. <sup>S1</sup> The following parameters were taken : $J = 3$ Hz, $k_{\text{dis}} = 11$ Hz. (a) The spectrum for small resonance frequency difference between A, X and B protons. Namely, $\Delta\omega = 30$ Hz is the difference between resonance frequencies for A (NH) and X (BH) protons. The dispersive signal for $\text{B}_2$ ( $\text{H}_2$ ) proton (4.6 ppm) is clearly visible. (b) $\Delta\omega$ is increased to 120 Hz, the dispersive signal for $\text{B}_2$ ( $\text{H}_2$ ) is almost disappeared. (c) $\Delta\omega$ is increased to match that for BorylCAT- $\text{H}_2$ (ca. 2700 Hz), dispersive $\text{H}_2$ signal so weak that is not visible. Our own written code in MATLAB was used to perform these calculations. ....	14
<b>Figure S10.</b> Potential energy surface scan of rotation of $\text{BH}_3$ moiety in BorylCAT- $\text{H}_2$ . ....	36
<b>Figure S11.</b> Optimized structures of BorylCAT- $\text{H}_2$ and the $\text{BH}_3$ rotational TS, respectively. Dihydrogen bond distances are shown in Ångstroms. ....	36
<b>Figure S12.</b> Calculated $J_{\text{NHHB}}$ coupling constants for conformers of BorylCAT- $\text{H}_2$ with $\text{C}_\text{N}\text{C}_\text{B}\text{BH}$ values ranging from 0 to $180^\circ$ .....	37

# 1 Full sets of variable temperature $^1\text{H}$ NMR spectra of AABs and para- $\text{H}_2$

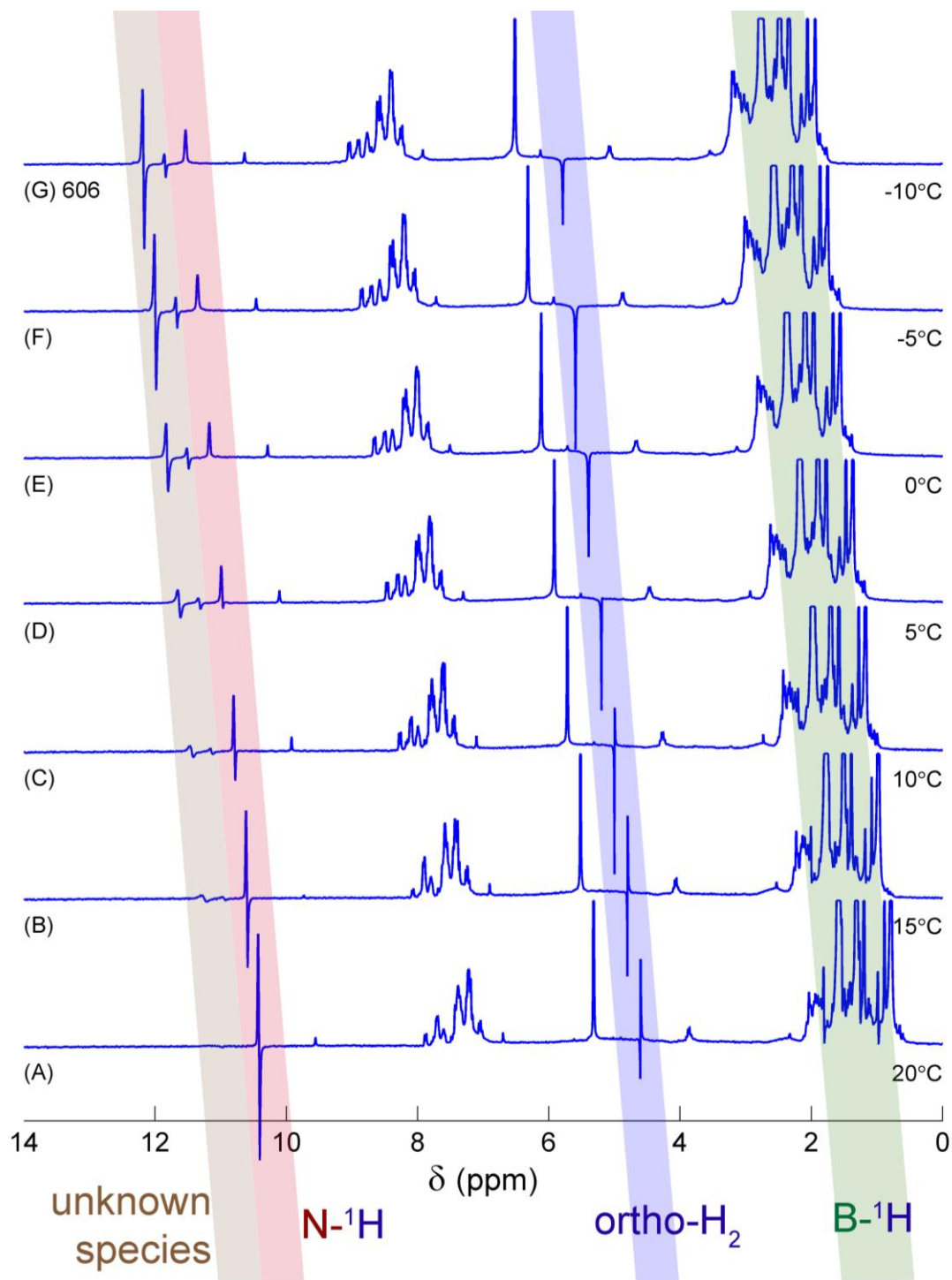


**Figure S1.**  $^{14}\text{N}$ -decoupled  $^1\text{H}$  NMR spectra acquired after para- $\text{H}_2$  bubbling through BorylCAT solution in methylene chloride- $\text{d}_2$ . The acquisition temperatures are shown in the figure.

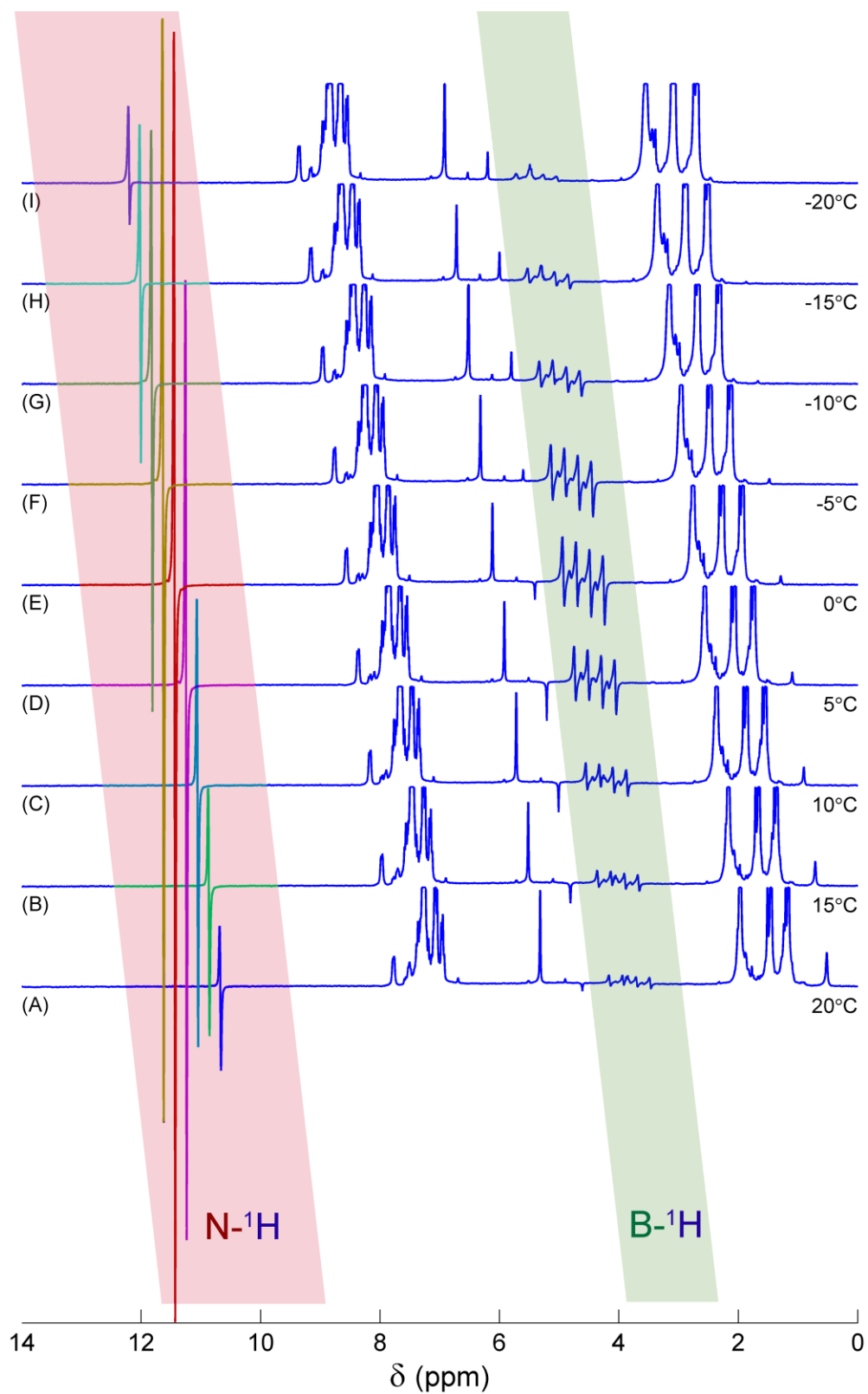


**Figure S2.**  $^{14}\text{N}$ -decoupled  $^1\text{H}$  NMR spectra acquired after para- $\text{H}_2$  bubbling through PhenylCAT solution in methylene chloride- $\text{d}_2$ . The acquisition temperatures are shown in the figure.

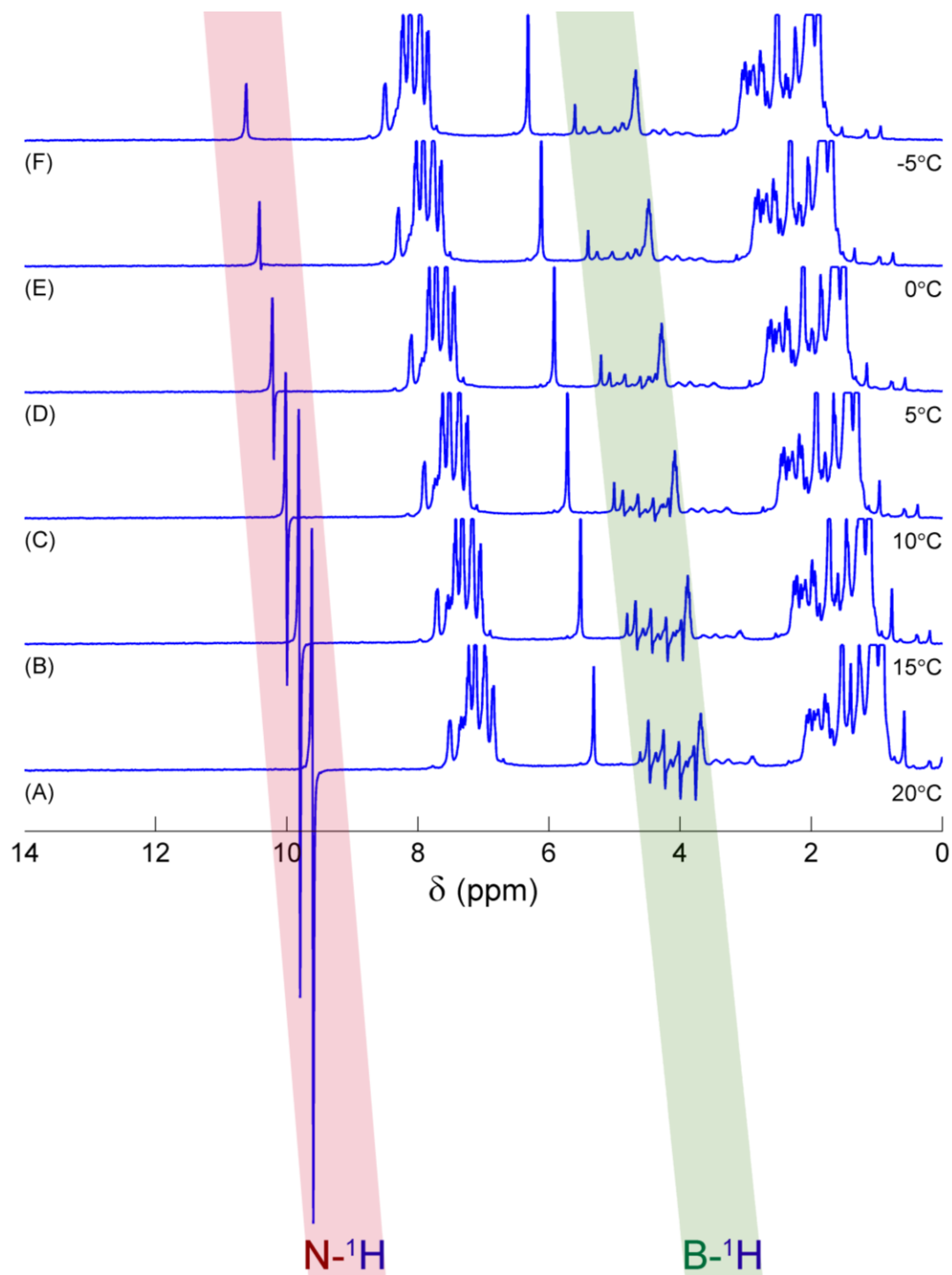


**Figure S3.**  $^{14}\text{N}$ -decoupled  $^1\text{H}$  NMR spectra acquired after para- $\text{H}_2$  bubbling through iPrPhenylCAT solution in methylene chloride- $\text{d}_2$ . The acquisition temperatures are shown in the figure.

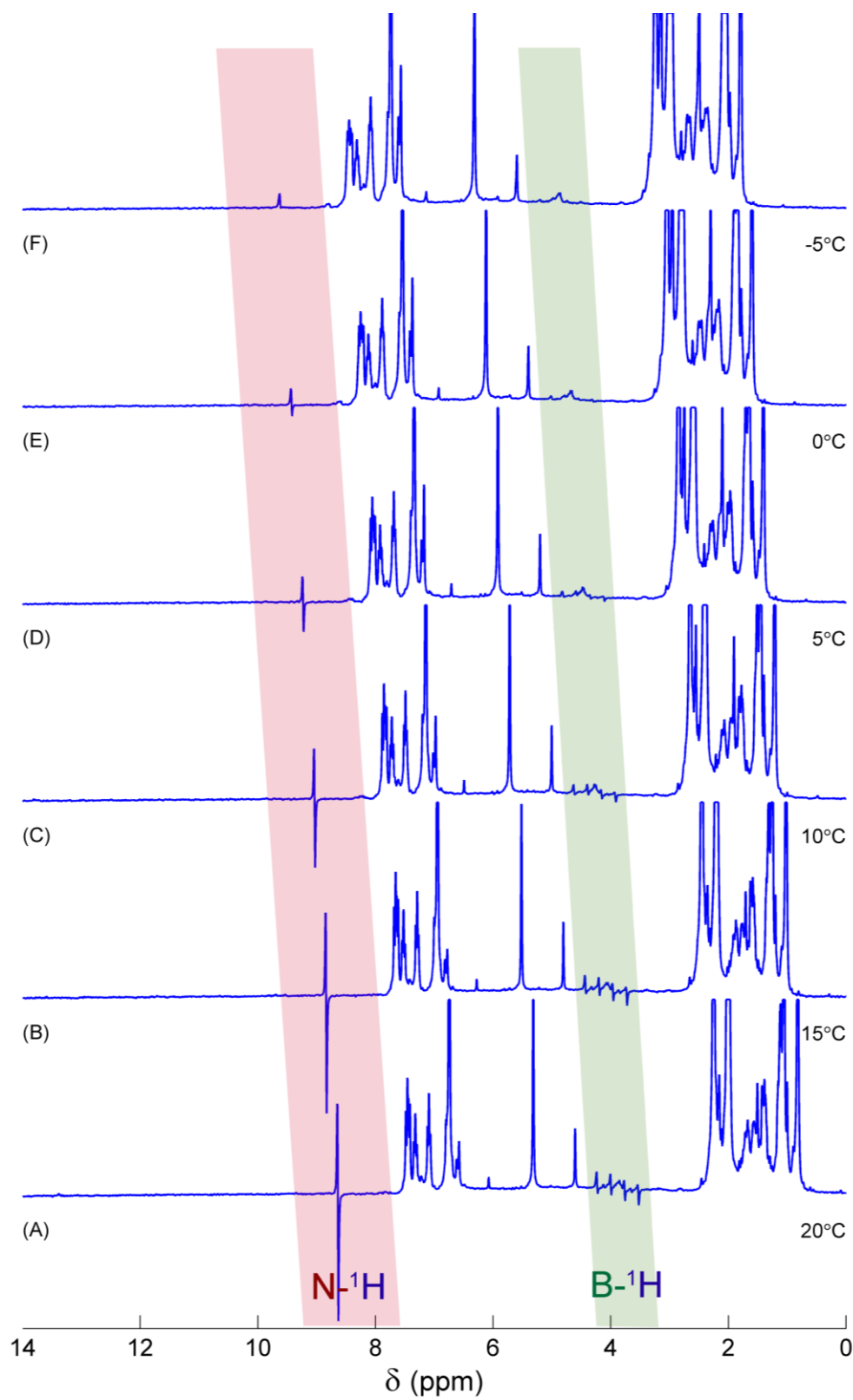


**Figure S4.**  $^{14}\text{N}$ -decoupled  $^1\text{H}$  NMR spectra acquired after para- $\text{H}_2$  bubbling through MesitylCAT solution in methylene chloride- $\text{d}_2$ . The acquisition temperatures are shown in the figure.

The NMR spectra were measured on a Bruker 300 MHz spectrometer with a standard variable temperature unit.

## 2 Kinetic and thermodynamic parameter determination

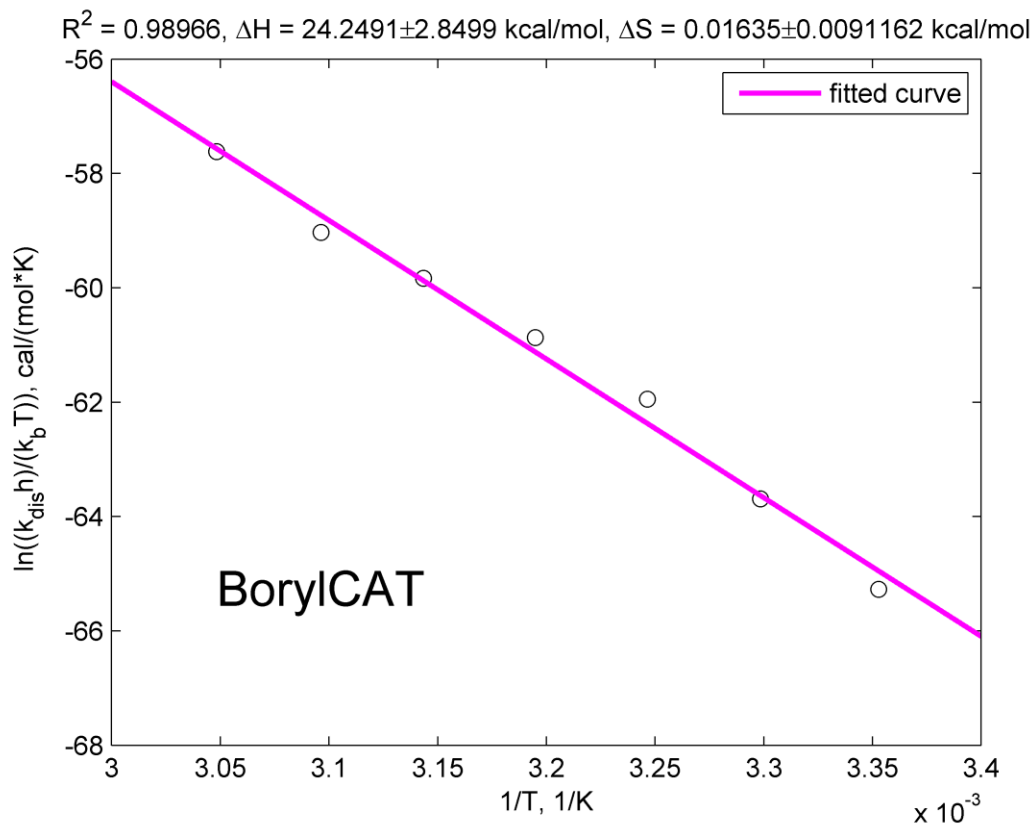


**Figure S5.** Eyring plot for BorylCAT compound. Experimental points are shown with circles and the linear fitting result is shown with magenta line. The parameters obtained from the fitting are shown in the title along with accuracy bounds of 95% probability.

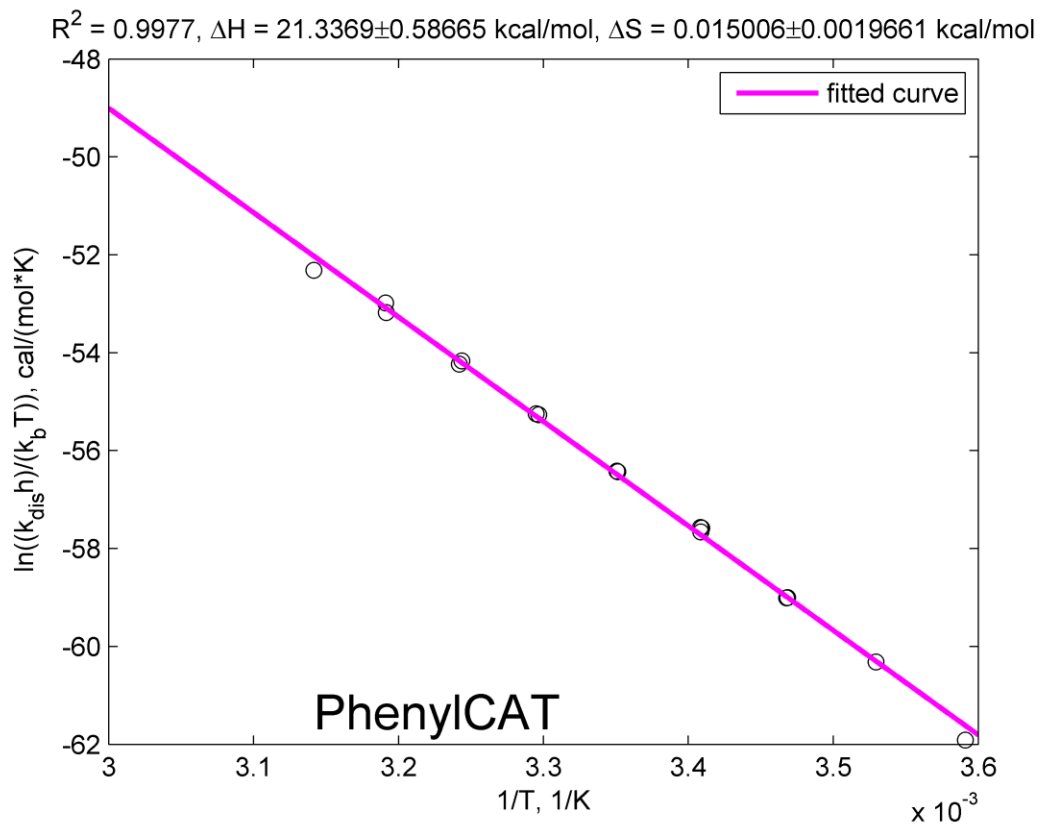


**Figure S6.** Eyring plot for PhenylCAT compound. Experimental points are shown with circles and the linear fitting result is shown with magenta line. The parameters obtained from the fitting are shown in the title along with accuracy bounds of 95% probability.

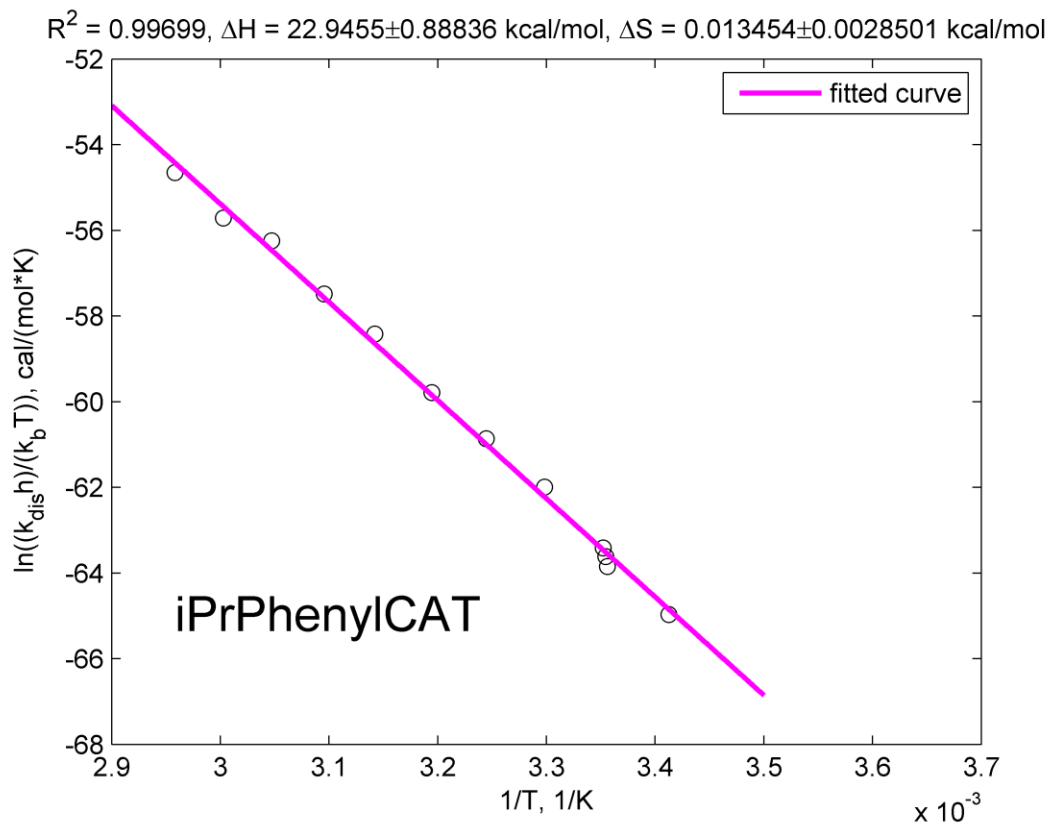


**Figure S7.** Eyring plot for iPrPhenylCAT compound. Experimental points are shown with circles and the linear fitting result is shown with magenta line. The parameters obtained from the fitting are shown in the title along with accuracy bounds of 95% probability.

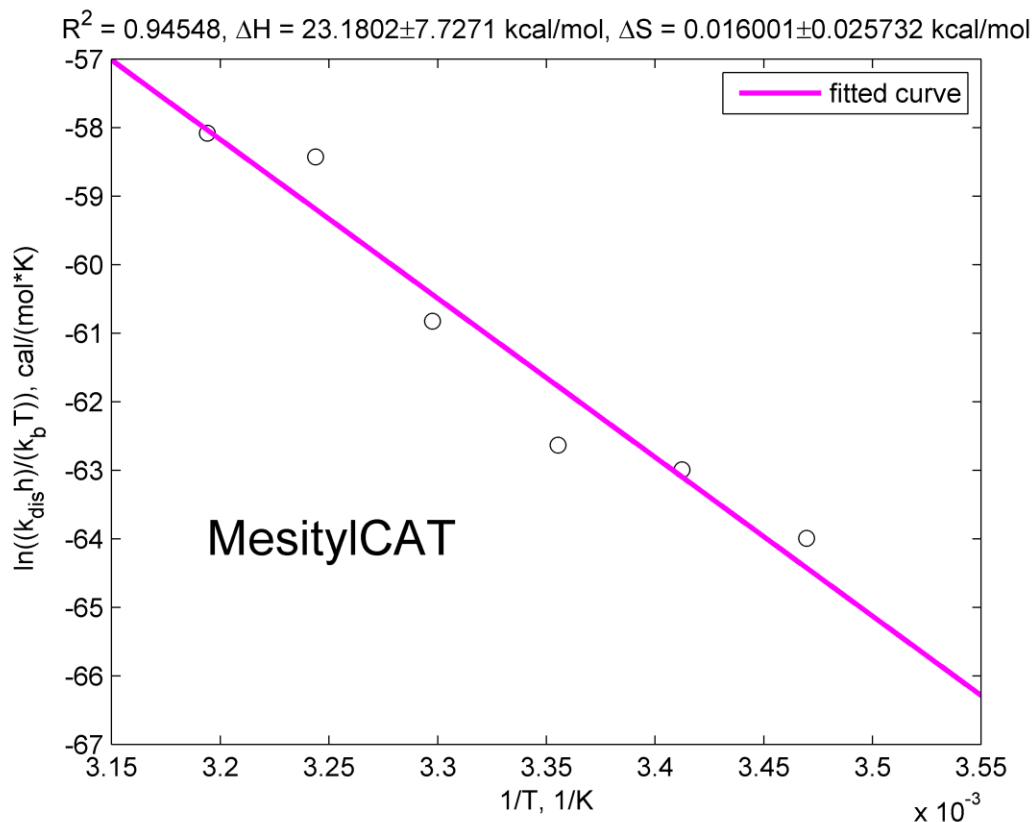


**Figure S8.** Eyring plot for MesitylCAT compound. Experimental points are shown with circles and the linear fitting result is shown with magenta line. The parameters obtained from the fitting are shown in the title along with accuracy bounds of 95% probability.

### 3 Actual values of PHIP signal attenuation factors calculated for the dimensionless parameters listed in Table 2 of the main text for the AABs under study

The contributions to the PHIP signal attenuation ruled by the three dimensionless parameters in the Table 2 can be considered separately. By using Equation 11 (main text) we define three attenuation factors as:

$$f_1 = \frac{2 \tan^{-1} \left( \left| \frac{\pi J}{1/T_2^* + k_{dis}} \right| \right)}{\pi}, f_2 = \frac{1}{1 + \frac{1}{K_c [H_2]_0}} \text{ and } f_3 = \frac{1}{1 + \frac{1}{k_{dis} T_1^*}}.$$

The numeric values of these factors are presented in Table S1.

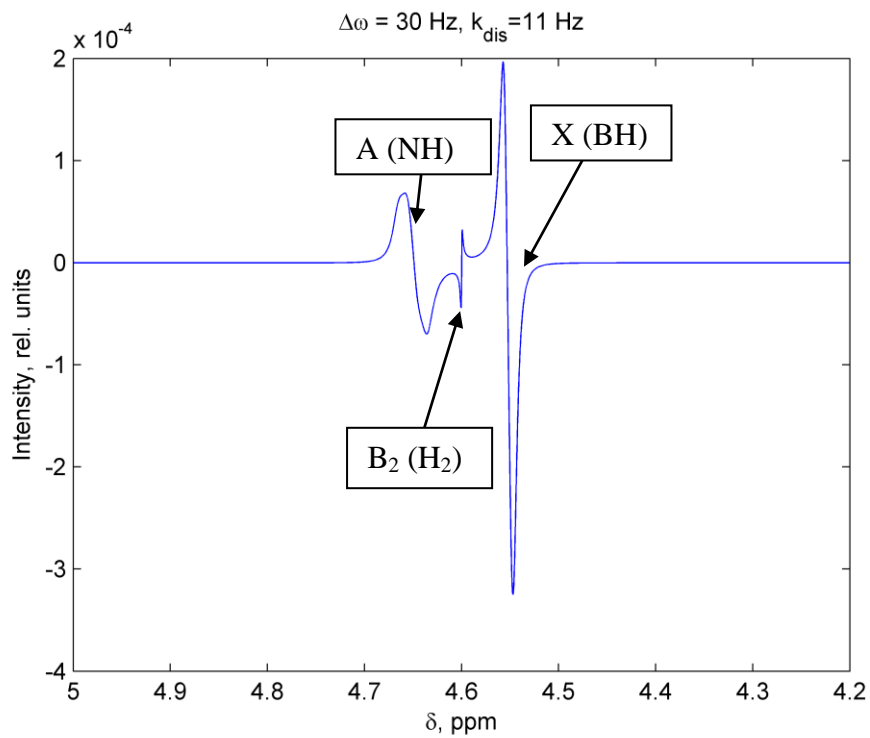
**Table S1.** PHIP signal attenuation factors calculated using characteristic dimensionless parameters from Table 2 (main text) for the AABs under study.

AAB	T, K	$f_1$	$f_2$	$f_3$	<sup>1</sup> Overall attenuation
BorylCAT	273	0.3440	0.5238	0.0004	0.00008
	283	0.3440	0.3333	0.0018	0.00021
	293	0.3440	0.2308	0.0058	0.00046
	303	–	0.0909	0.0440	–
PhenylCAT	273	0.4295	0.9861	0.0049	0.00206
	283	0.4665	0.9545	0.0427	0.01900
	293	0.4665	0.9000	0.1834	0.07699
	303	–	0.7500	0.4705	–
iPrPhenylCAT	273	0.3440	0.9697	0.0002	0.00007
	283	0.3888	0.9231	0.0011	0.00038
	293	0.4295	0.8333	0.0045	0.00161
	303	–	0.6667	0.0259	–
MesitylCAT	273	0.3888	0.1228	0.0006	0.00003
	283	0.4665	0.0476	0.0026	0.00006
	293	0.4665	0.0196	0.0139	0.00012
	303	–	0.0099	0.0437	–

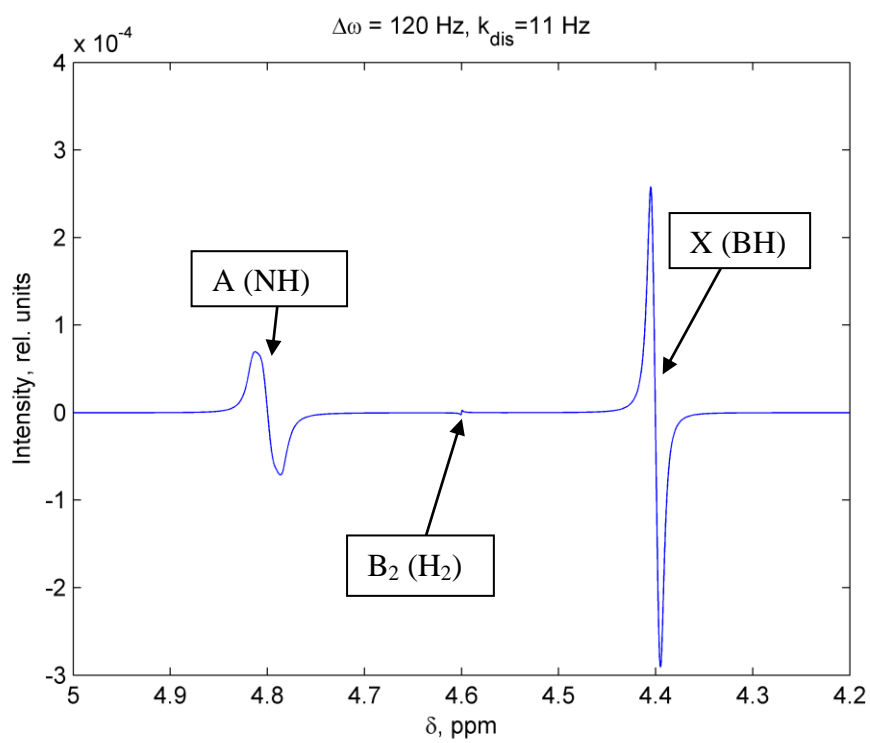
<sup>1</sup>Product of  $f_1$ ,  $f_2$  and  $f_3$ .

#### 4 Numerical simulations of $^1\text{H}$ NMR spectra with presence of chemical exchange

(a)



(b)



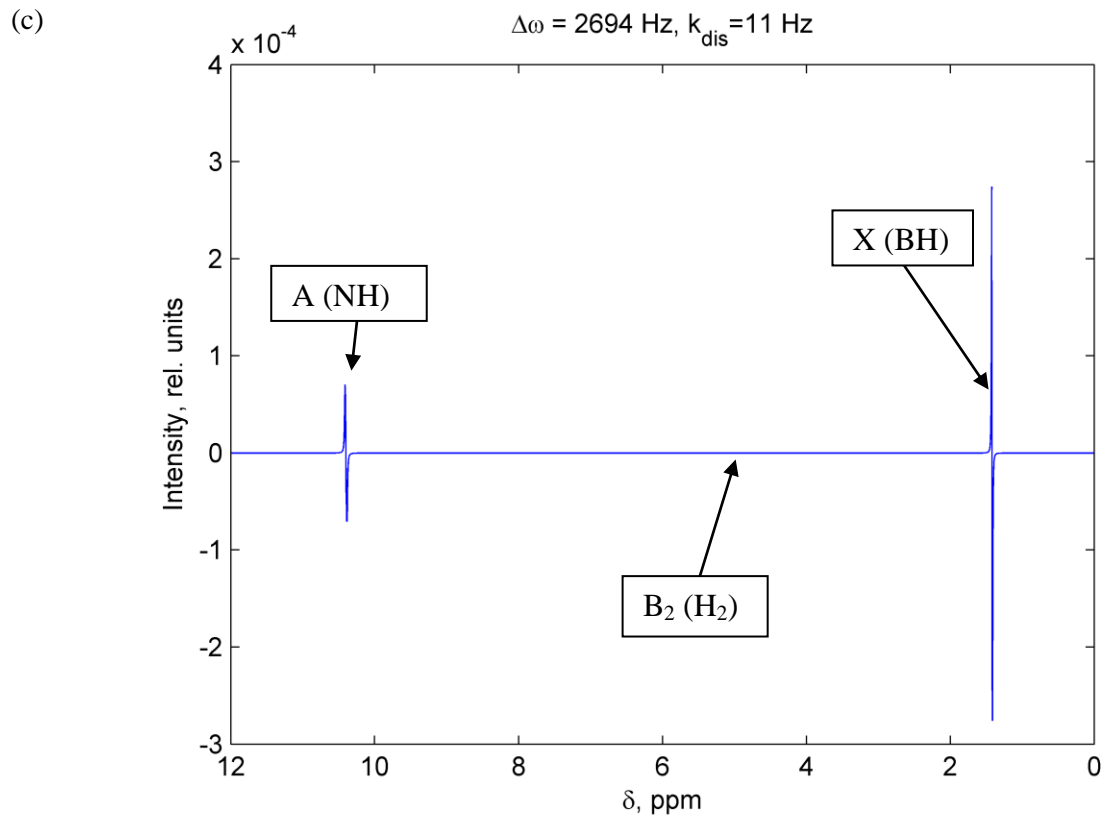


**Figure S9.** Simulation results of  $^1\text{H}$  NMR spectra for  $\text{AX}_3$  spin system (a model for BorylCAT- $\text{H}_2$ ), in which a pair of AX protons exchanges chemically with  $\text{B}_2$  spin system (a model for molecular  $\text{H}_2$ ). The simulation includes numerical propagation of the density operator under the action of coherent nuclear spin Hamiltonian superoperator as well as kinetic and uncorrelated relaxation Liouvillian operators.<sup>S1</sup> The following parameters were taken :  $J = 3 \text{ Hz}$ ,  $k_{\text{dis}} = 11 \text{ Hz}$ . (a) The spectrum for small resonance frequency difference between A, X and B protons. Namely,  $\Delta\omega = 30 \text{ Hz}$  is the difference between resonance frequencies for A (NH) and X (BH) protons. The dispersive signal for  $\text{B}_2$  ( $\text{H}_2$ ) proton (4.6 ppm) is clearly visible. (b)  $\Delta\omega$  is increased to 120 Hz, the dispersive signal for  $\text{B}_2$  ( $\text{H}_2$ ) is almost disappeared. (c)  $\Delta\omega$  is increased to match that for BorylCAT- $\text{H}_2$  (ca. 2700 Hz), dispersive  $\text{H}_2$  signal so weak that is not visible. Our own written code in MATLAB was used to perform these calculations.

## 5 Derivation of analytical formula for $I_z I_z$ amplitude accommodated in AAB- $H_2$ molecules under reversible chemical exchange conditions and para- $H_2$ bubbling

For the sake of simplicity, we assumed two spin-1/2 system for the coupled NH and BH protons in AAB- $H_2$ . This assumption is good for PhenylCAT, iPrPhenylCAT and MesitylCAT, while in the case of BorylCAT this assumption ignores the presence of two extra protons in  $BH_3$  group. Assuming the free rotation  $BH_3$  group, the three protons are magnetically equivalent and the two spin system assumption should also give acceptable results for these compound. The B-H and N-H couplings were also ignored as the fast relaxation of quadrupolar  $^{11}B$  ( $^{10}B$ ) and  $^{14}N$  nuclei led to the collapse of the multiplet structure in  $^1H$  NMR spectra of the AAB- $H_2$  adducts.

First we write coherent spin Liouvillian operator in the basis of shift ( $I^+$  and  $I^-$ ) and  $z$  projection operators ( $I_z$ ) by using standard procedures.<sup>S1</sup> The 0-quantum operators block for the coherent Liouvillian operator reads

$$\hat{L}_0 = \begin{pmatrix} 2\pi(\omega_1 - \omega_2) & 0 & 0 & J\pi & -J\pi & 0 \\ 0 & 2\pi(\omega_2 - \omega_1) & 0 & -J\pi & J\pi & 0 \\ 0 & 0 & 0 & 0 & 0 & 0 \\ J\pi & -J\pi & 0 & 0 & 0 & 0 \\ -J\pi & J\pi & 0 & 0 & 0 & 0 \\ 0 & 0 & 0 & 0 & 0 & 0 \end{pmatrix}, \quad (1)$$

where  $\omega_1$  and  $\omega_2$  are resonance frequencies for spin 1 and spin 2, respectively and  $J$  is the scalar spin-spin coupling constant between the spins. The normalized basis operators are following:

$$Basis^{\hat{L}_0} = \left\{ \hat{I}_1^- \hat{I}_2^+, \hat{I}_1^+ \hat{I}_2^-, 2\hat{I}_{1z} \hat{I}_{2z}, \hat{I}_{1z}, \hat{I}_{2z}, \frac{\hat{I}}{2} \right\}. \quad (2)$$

The incoherent dynamics due to the presence of chemical exchange is determined by the following kinetic operator,

$$\hat{K}0 = \begin{pmatrix} -k_{\text{dis}} & 0 & 0 & 0 & 0 & -\frac{k_{\text{dis}}}{2} \\ 0 & -k_{\text{dis}} & 0 & 0 & 0 & -\frac{k_{\text{dis}}}{2} \\ 0 & 0 & -k_{\text{dis}} & 0 & 0 & -\frac{k_{\text{dis}}}{2} \\ 0 & 0 & 0 & -k_{\text{dis}} & 0 & 0 \\ 0 & 0 & 0 & 0 & -k_{\text{dis}} & 0 \\ 0 & 0 & 0 & 0 & 0 & 0 \end{pmatrix} \quad (3)$$

where  $k_{\text{dis}}$  is the AAB-H<sub>2</sub> dissociation rate constant. This form of the kinetic operators takes care about depletion of all non-equilibrium nuclear spin orders (diagonal elements) and the enrichment of para-H<sub>2</sub> nuclear spin order ( $(-\hat{I}_1^- \hat{I}_2^+ - \hat{I}_1^+ \hat{I}_2^-)/2 - \hat{I}_{1z} \hat{I}_{2z}$ , source terms in the last column) because of the chemical exchange which lets the para-H<sub>2</sub> nuclear spin order in. The unity operator ( $\hat{\mathbb{I}}/2$ ) amplitude is assumed unchanged (actually set 1) as we assume chemical equilibrium to be reached, implying that the concentration of AAB-H<sub>2</sub> is preserved. Finally, the solution of Liouville-von Neumann equation provides time dependence of the 0-quantum nuclear spin order in the form of

$$\rho(t) = \rho_0 \exp((\hat{K}0 - i\hat{L}0)t), \quad (4)$$

where  $\rho(t)$  and  $\rho_0$  are column vectors of the time-dependent and initial amplitudes of basis operators, respectively. The elimination (averaging) of all oscillatory terms from the expressions for  $\hat{I}_1^- \cdot \hat{I}_2^+$ ,  $\hat{I}_1^+ \cdot \hat{I}_2^-$  and  $2\hat{I}_{1z} \cdot \hat{I}_{2z}$  operator amplitudes provides the following stationary solution

$$\left\{ A(\hat{I}_1^- \cdot \hat{I}_2^+), A(\hat{I}_1^+ \cdot \hat{I}_2^-), A(2\hat{I}_{1z} \cdot \hat{I}_{2z}) \right\}_{\text{stationary}} = \left\{ -\frac{1}{2} \frac{J^2 + k_{\text{dis}}^2 / (2\pi)^2 - i\Delta\omega k_{\text{dis}} / (2\pi)}{J^2 + k_{\text{dis}}^2 / (2\pi)^2 + \Delta\omega^2}, -\frac{1}{2} \frac{J^2 + k_{\text{dis}}^2 / (2\pi)^2 + i\Delta\omega k_{\text{dis}} / (2\pi)}{J^2 + k_{\text{dis}}^2 / (2\pi)^2 + \Delta\omega^2}, -\frac{1}{2} \right\}, \quad (5)$$

where  $\Delta\omega = \omega_1 - \omega_2$ . We need to consider the real part of the amplitudes to estimate the conversion of the para-H<sub>2</sub> nuclear spin order ( $(-\hat{I}_1^- \cdot \hat{I}_2^+ - \hat{I}_1^+ \cdot \hat{I}_2^-)/2 - \hat{I}_{1z} \hat{I}_{2z}$ ) to only  $\hat{I}_{1z} \hat{I}_{2z}$  nuclear spin order, as the amplitudes of both of these operators are real. Thus, the subtraction of

the real part for  $\hat{I}_1^- \cdot \hat{I}_2^+$  or  $\hat{I}_1^+ \cdot \hat{I}_2^-$  amplitudes (they are equal) from unity provides the measure of the conversion varying from 0 to 1:

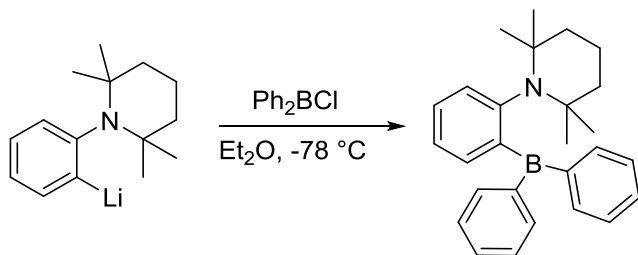
$$f_{zz} = \frac{\Delta\omega^2}{\Delta\omega^2 + J^2 + \left(\frac{k_{dis}}{2\pi}\right)^2}. \quad (6)$$

This measure is referred in main text as  $\hat{I}_{1z} \cdot \hat{I}_{2z}$  amplitude factor taking into account the features of spin dynamics which leads to the conversion of the parahydrogen nuclear spin order into the two spin longitudinal nuclear spin order  $\hat{I}_{1z} \cdot \hat{I}_{2z}$ .

$f_{zz}$  values for ABBs compounds studied in this work were close to unity as soon as  $\Delta\omega$  was high ( $> 1.5$  kHz), while  $J$  ( $< 8$  Hz) and  $k_{dis}$  ( $< 10$  Hz) were low. The calculation using the typical values gives  $f_{zz} = 1500^2 / (1500^2 + 8^2 + (10/(2\pi))^2) = 0.99997$ , meaning that the conversion from the singlet spin order to  $\hat{I}_{1z} \cdot \hat{I}_{2z}$  is almost quantitative.

## 6 Preparation of *ansa*-aminoboranes

### 6.1 1-(2-(Diphenylboryl)phenyl)-2,2,6,6-tetramethylpiperidine (PhenylCAT)



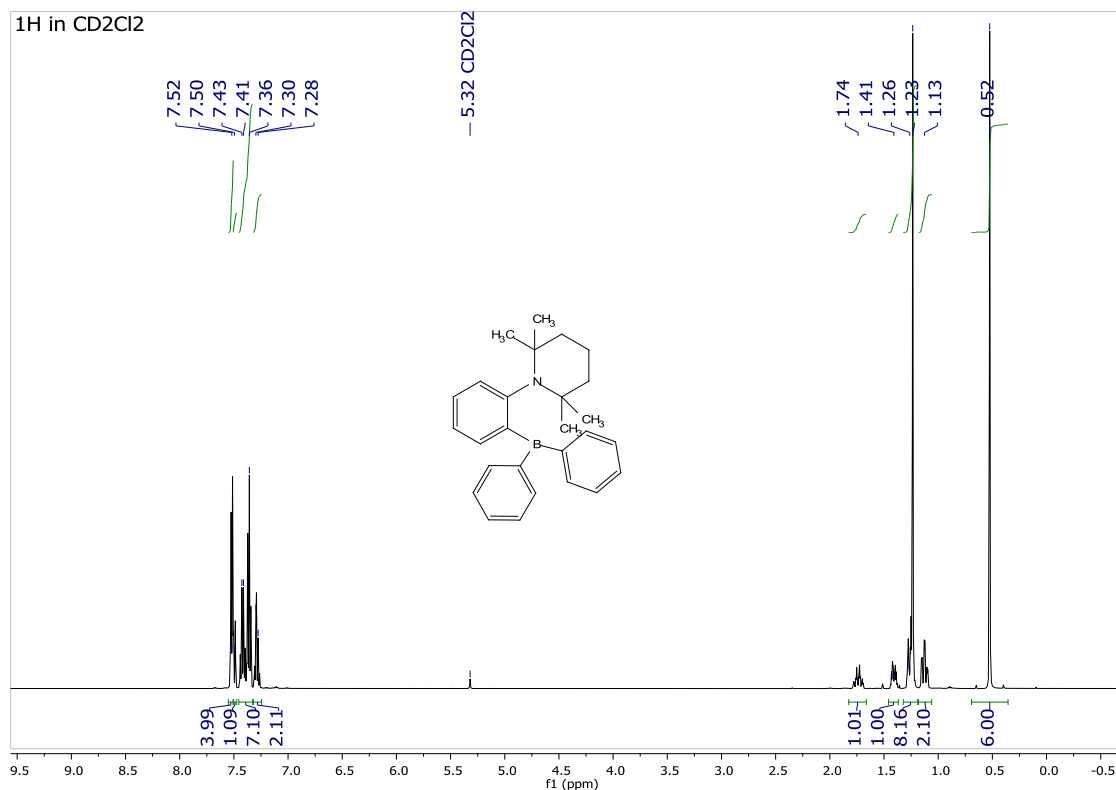
A solution of 0.557 g of (2-(2,2,6,6-tetramethylpiperidin-1-yl)phenyl)lithium<sup>S2</sup> (2.5 mmol) in 6 ml of diethyl ether was prepared in a 25 ml Schlenk tube and cooled to  $-78$  °C. Using syringe, a solution of 0.500 g of chlorodiphenylborane (2.5 mmol) in 5 ml of diethyl ether was added dropwise to the stirred solution of the lithium salt within 10 min. The mixture was allowed to warm to room temperature and was left stirred overnight. The solvent was removed under

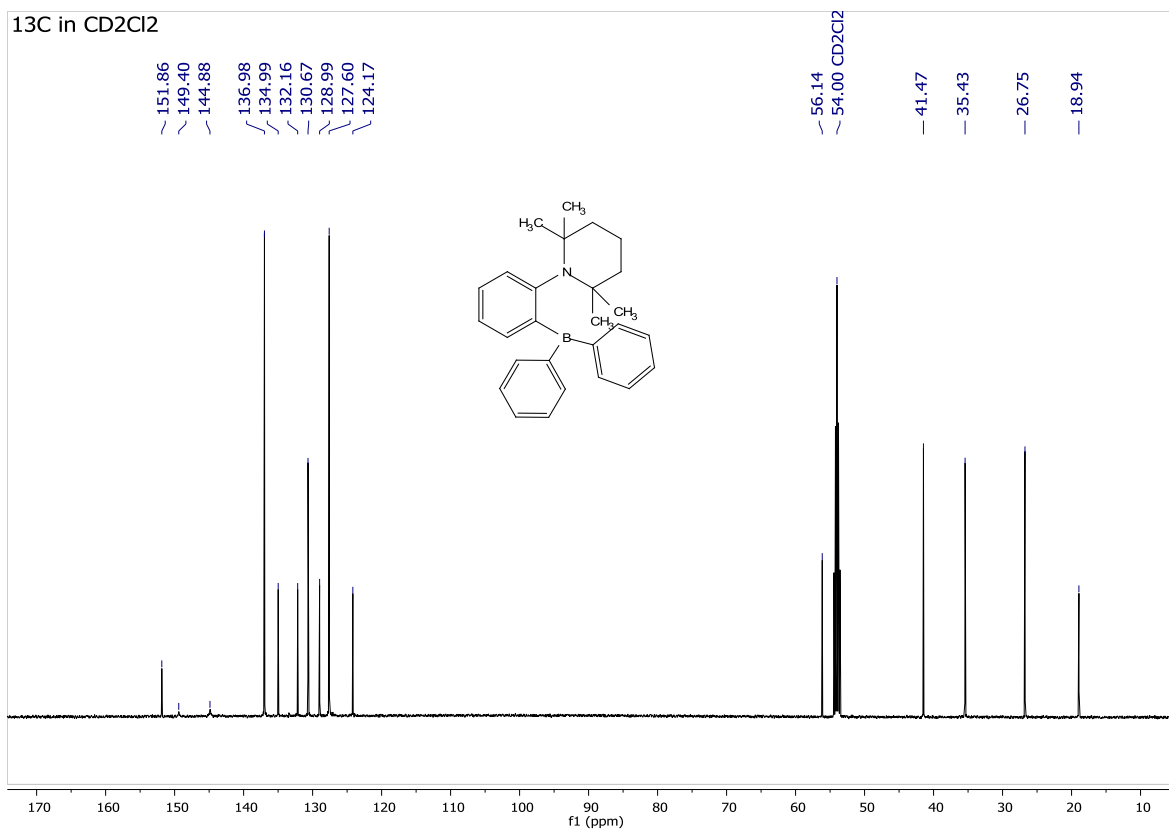
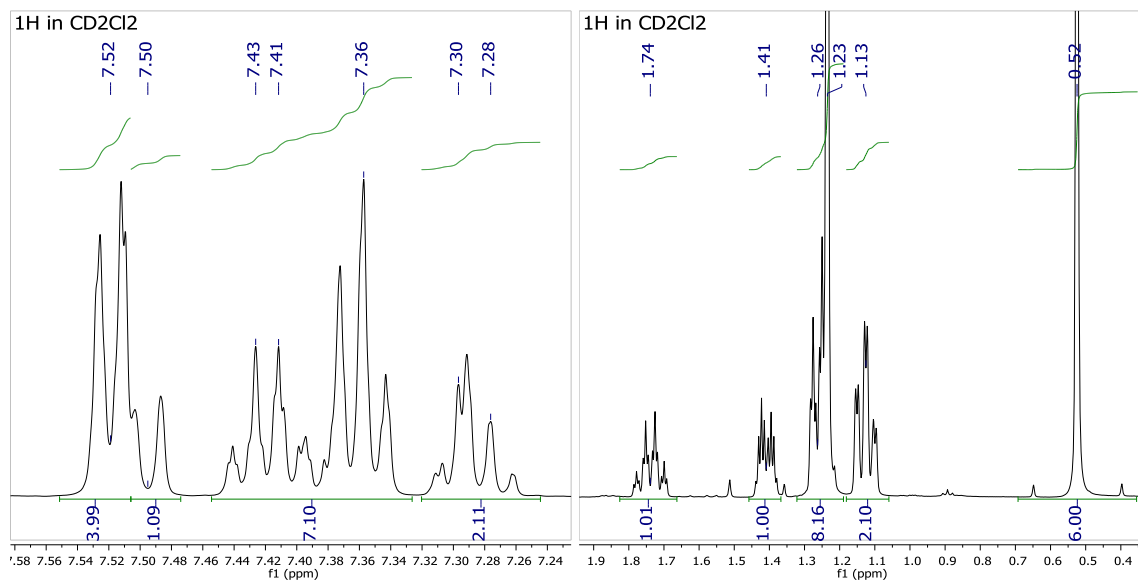
reduced pressure to dryness. The residue was suspended in 10 ml of toluene, was filtered, and the filter cake was washed with additional portions (5x1 ml) of toluene. The combined filtrate was evaporated to dryness yielding a yellow solid of crude aminoborane in quantitative yield. Recrystallization from 100 ml of the 20:1 hexane-toluene mixture gave 0.404 g (42.5%) of pure target compound as large colorless crystals.

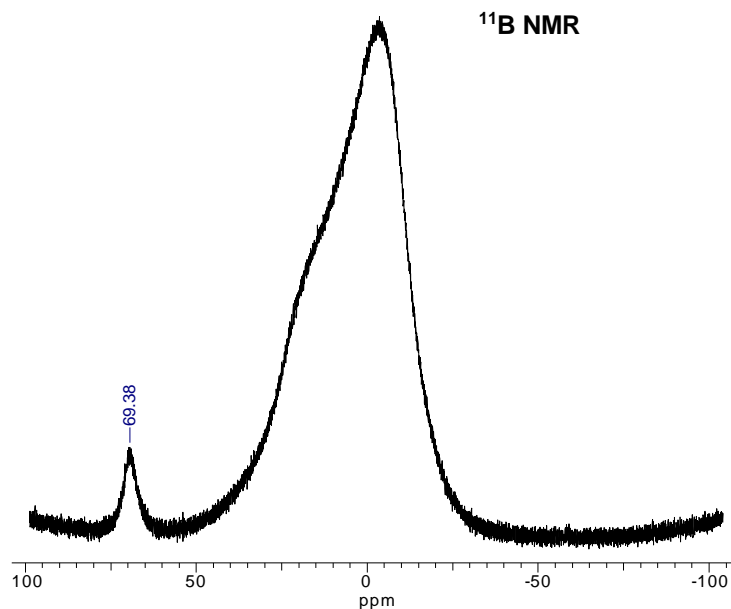
$^1\text{H}$  NMR (500 MHz,  $\text{CD}_2\text{Cl}_2$ ,  $\delta$ , ppm): 7.52 (m, 4H), 7.50 (d,  $J = 8.1$  Hz, 1H), 7.45–7.33 (m, 7H), 7.32–7.25 (m, 2H), 1.74 (dtt,  $J = 13.5, 13.0, 3.6$  Hz, 1H), 1.41 (dq,  $J = 13.9, 3.9$  Hz, 1H), 1.26 (dt,  $J = 12.9, 3.9$  Hz, 2H), 1.23 (s, 6H), 1.13 (td,  $J = 12.7, 3.8$  Hz, 2H), 0.52 (s, 6H).

$^{13}\text{C}$  NMR (126 MHz,  $\text{CD}_2\text{Cl}_2$ ,  $\delta$ , ppm): 151.86 (TMP-C), 149.40 (B- $\text{C}_{\text{PhTMP}}$ ), 144.88 (B- $\text{C}_{\text{Ph}}$ ), 136.98 (Ph), 134.99 ( $\text{C}_6\text{H}_4$ ), 132.16 ( $\text{C}_6\text{H}_4$ ), 130.67 (Ph), 128.99 ( $\text{C}_6\text{H}_4$ ), 127.60 (Ph), 124.17 ( $\text{C}_6\text{H}_4$ ), 56.14 ( $\text{NCMe}_2\text{CH}_2$ ), 41.47, 35.43, 26.75, 18.94 ( $\text{CH}_2\text{CH}_2\text{CH}_2$ ).

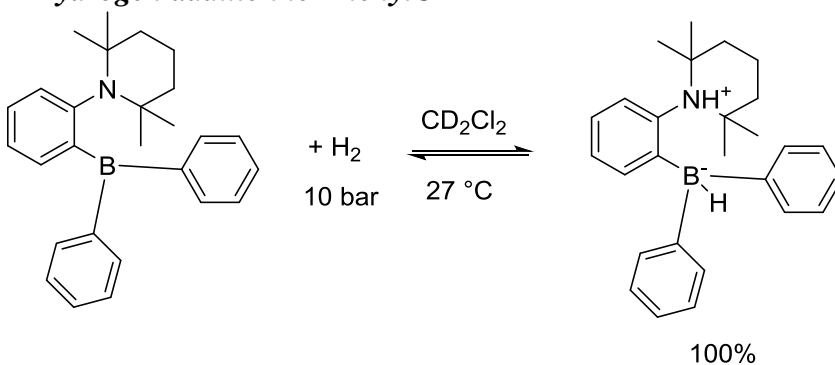
$^{11}\text{B}$  NMR (160 MHz,  $\text{CD}_2\text{Cl}_2$ ,  $\delta$ , ppm): 69.4 (br. s).







## 6.2 Hydrogen addition to PhenylCAT



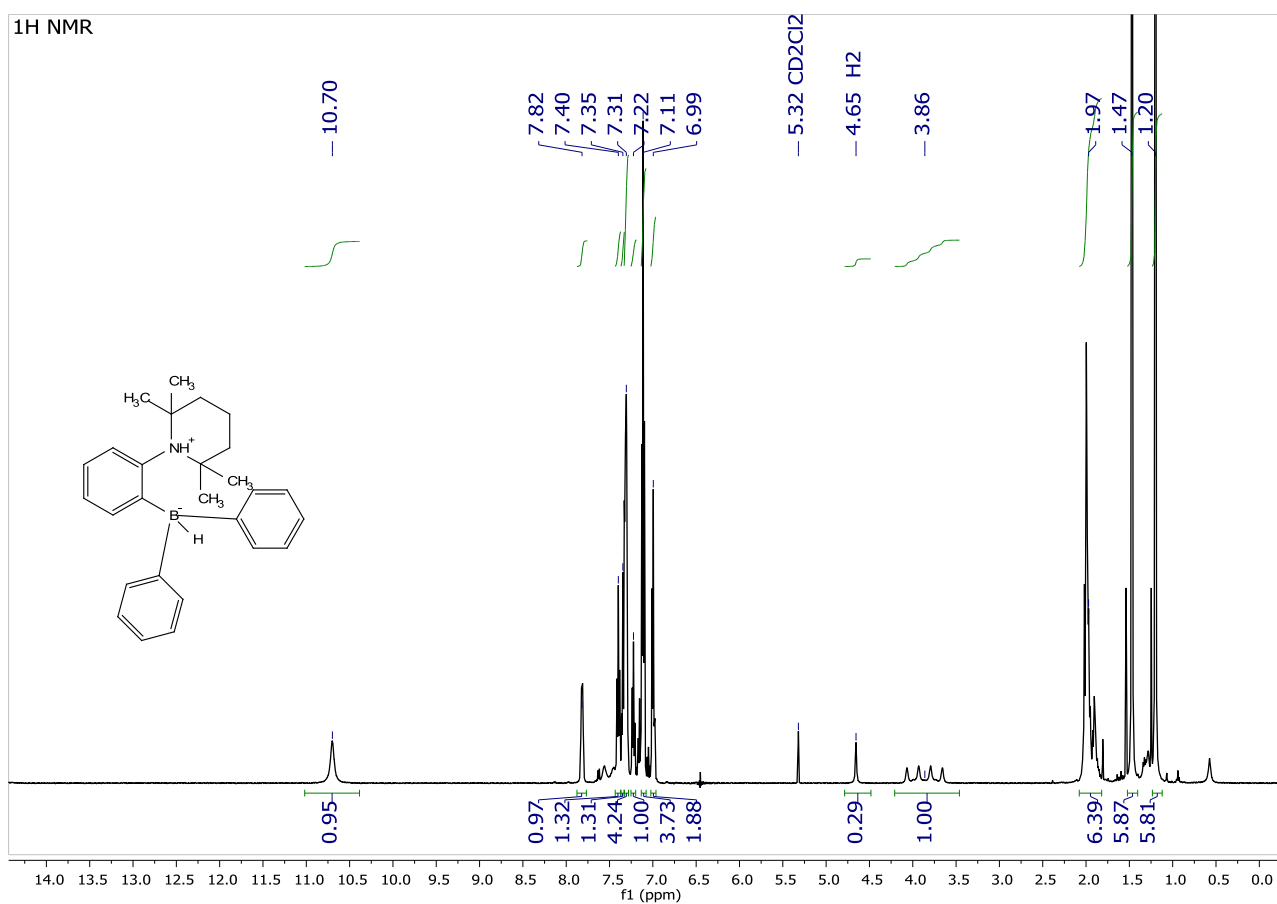
30 mg (0.078 mmol) of **PhenylCAT** was dissolved in 0,3 ml of  $\text{CD}_2\text{Cl}_2$ . The solution was placed into a gas-tight heavy wall NMR tube (5 mm Heavy Wall Precision Quick Pressure Valve NMR Sample Tube by Wilmad, 522-QPV-7, 13.8 bar max working pressure) and then it was filled with hydrogen to 10 bar by three refill-release cycles.

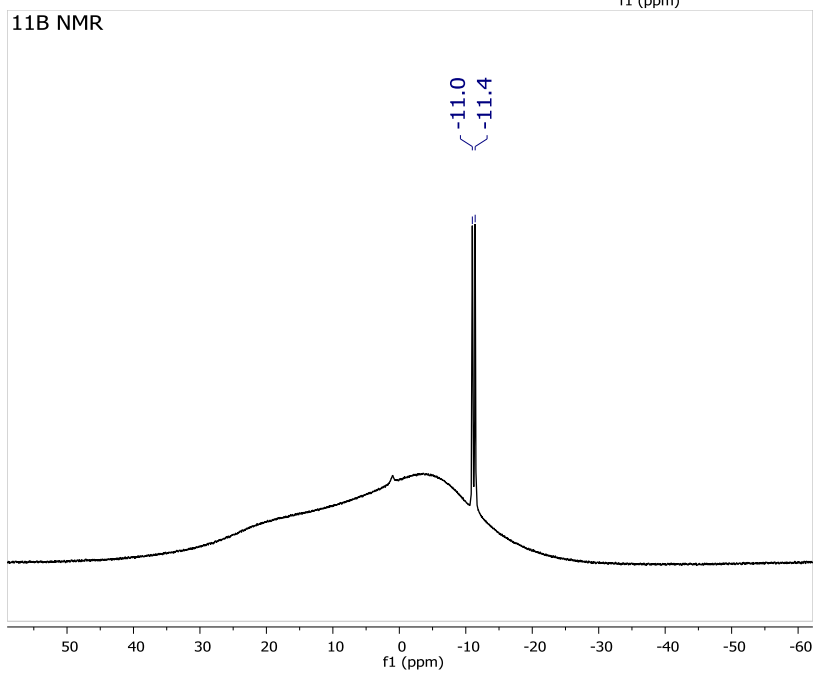
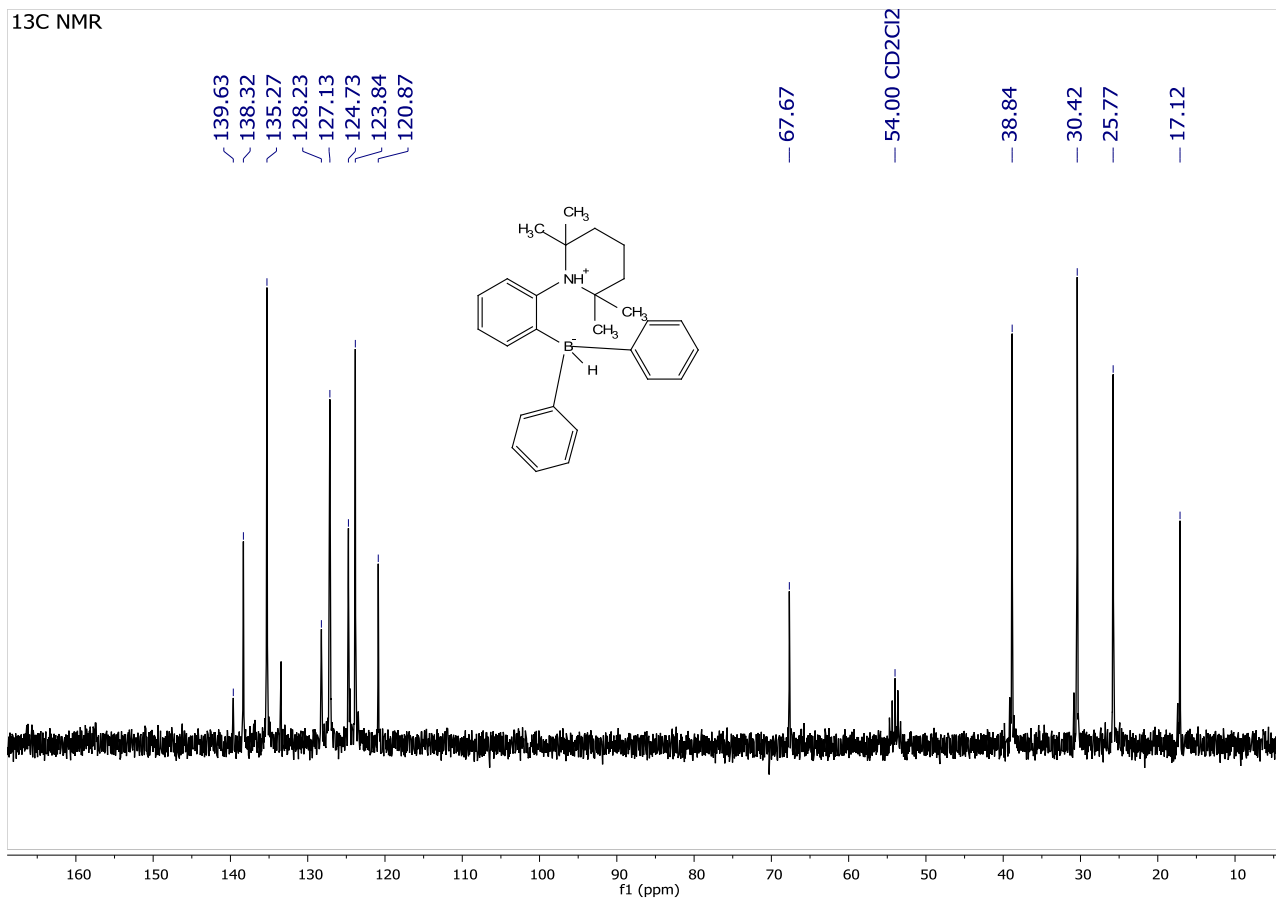
After 10 minutes the sample was analyzed by  $^1\text{H}$ ,  $^{11}\text{B}$ , and  $^{13}\text{C}$  NMR spectroscopy that revealed complete conversion of the aminoborane into its hydrogen adduct. Hydrogen was then released from the tube and the open tube was left standing at room temperature under an argon atmosphere for 24 h. A repeated  $^1\text{H}$  NMR analysis revealed a mixture of **PhenylCAT** and its  $\text{H}_2$  adduct in a ~70:30 ratio.

$^1\text{H}$  NMR (500 MHz,  $\text{CD}_2\text{Cl}_2$ ,  $\delta$ , ppm): 10.70 (s, NH), 7.82 (d,  $J = 6.7$  Hz, 1H), 7.40 (t,  $J = 7.2$  Hz, 1H), 7.35 (m, 1H), 7.31 (m, 4H), 7.22 (t,  $J = 7.7$  Hz, 1H), 7.11 (t,  $J = 7.5$  Hz, 4H), 6.99 (m, 2H), 3.86 (q,  $J = 68.3$  Hz, 1H, BH), 1.97 (m, 6H), 1.47 (s, 6H,  $\text{Me}_{\text{TMP}}$ ), 1.20 (s, 6H,  $\text{Me}_{\text{TMP}}$ ).

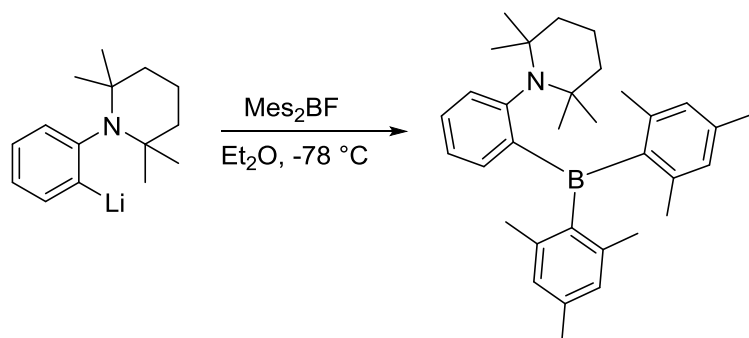
$^{13}\text{C}$  NMR (75 MHz,  $\text{CD}_2\text{Cl}_2$ ,  $\delta$ , ppm): 139.63, 138.32, 135.27 ( $\text{CH}_{\text{Ph}}$ ), 128.23, 127.13 ( $\text{CH}_{\text{Ph}}$ ), 124.73, 123.84 ( $\text{CH}_{\text{Ph}}$ ), 120.87, 67.67 ( $\text{NC}_{\text{TMP}}$ ), 38.84 ( $\text{CH}_2\text{CH}_2\text{CH}_2$ ), 30.42 ( $\text{Me}_{\text{TMP}}$ ), 25.77 ( $\text{Me}_{\text{TMP}}$ ), 17.12 ( $\text{CH}_2\text{CH}_2\text{CH}_2$ ).

$^{11}\text{B}$  (160 MHz,  $\text{C}_6\text{D}_6$ ,  $\delta$ , ppm): -11.20 (d,  $J = 68.2$  Hz)





### 6.3 1-(2-(Dimesitylboryl)phenyl)-2,2,6,6-tetramethylpiperidine (MesitylCAT)

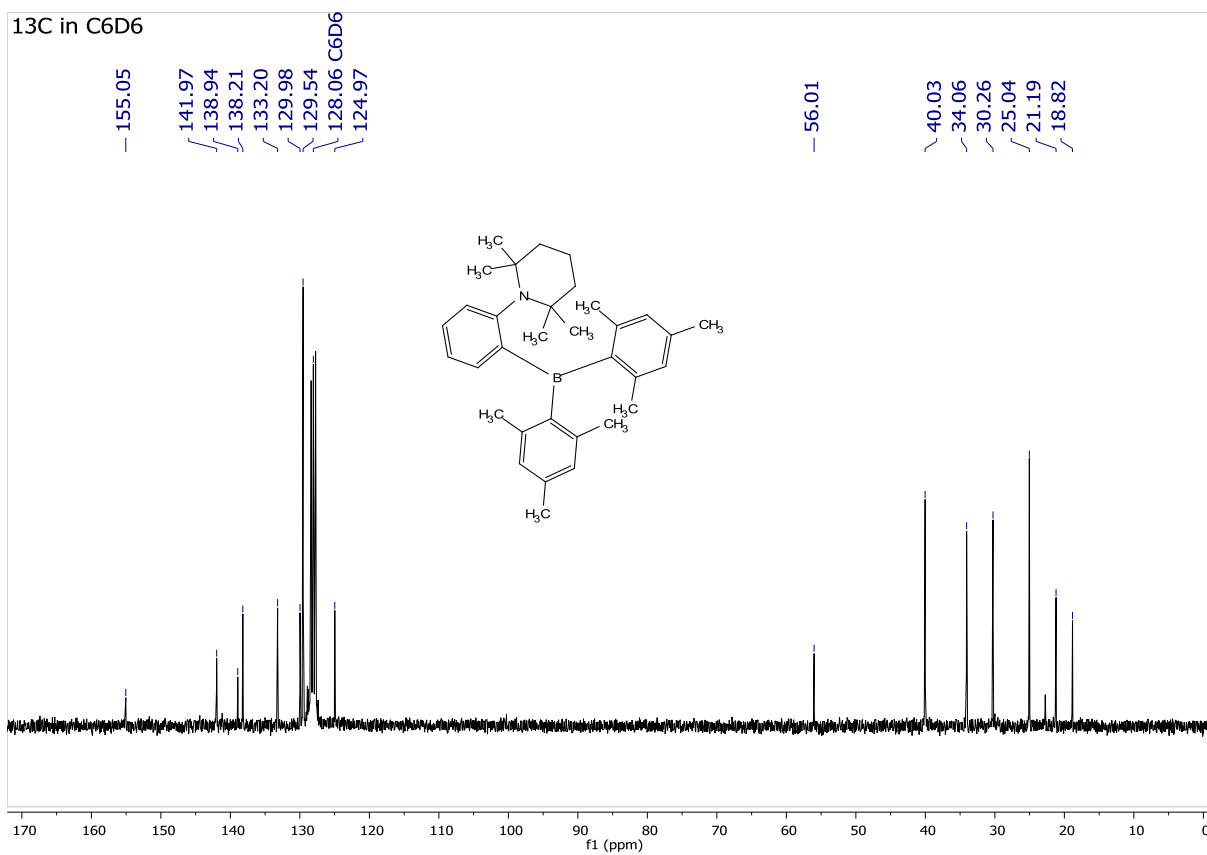
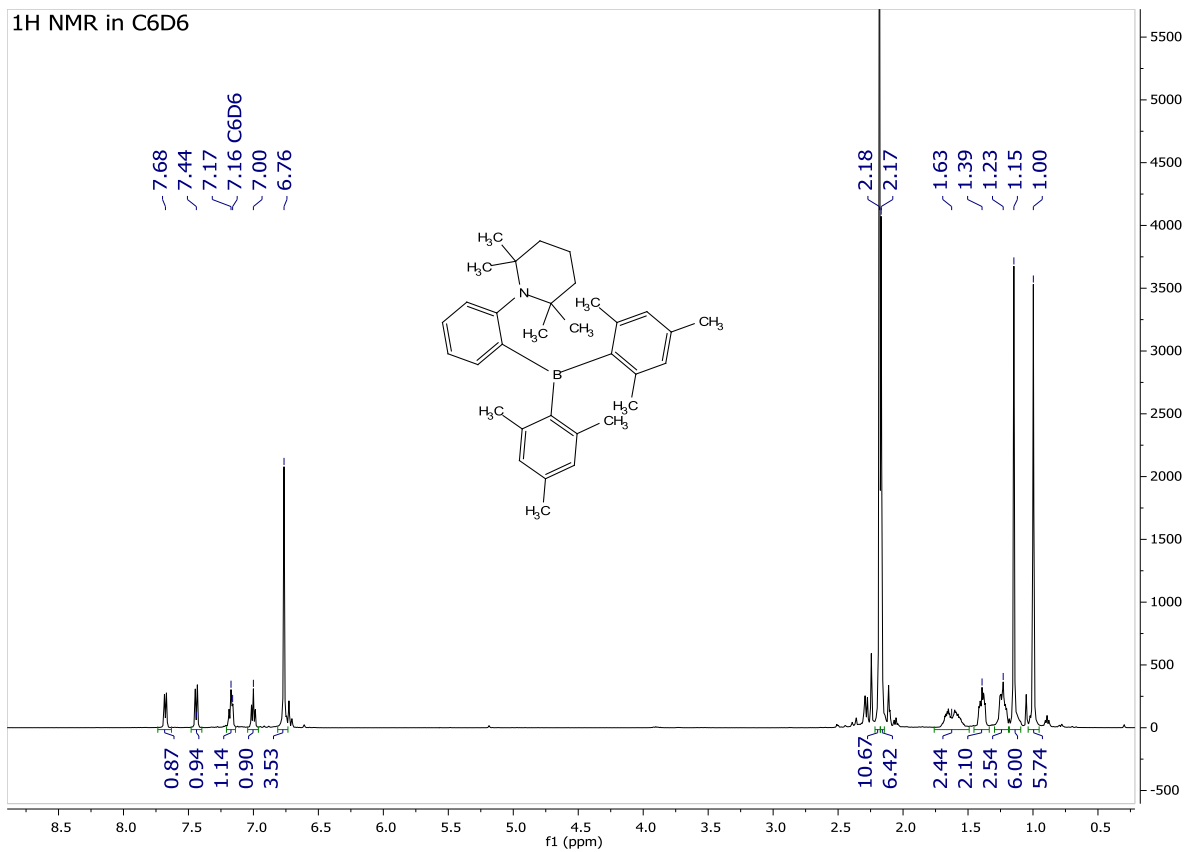


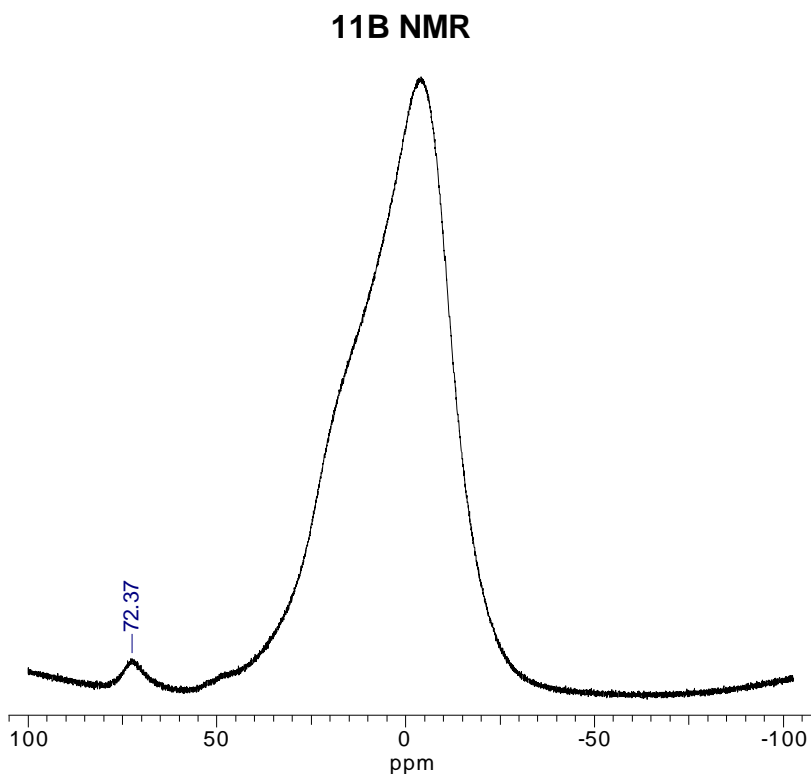
The compound was prepared similarly to 1-(2-(diphenylboryl)phenyl)-2,2,6,6-tetramethylpiperidine starting from 0.416 g of (2-(2,2,6,6-tetramethylpiperidin-1-yl)phenyl)lithium (1.86 mmol) and 0.500 g of fluorodimesitylborane (1.86 mmol). Evaporation of the toluene filtrate to dryness yielded 0.866 g (100%) of yellow oil that slowly crystallized upon standing. The compound was used without further purification.

<sup>1</sup>H (500 MHz, C<sub>6</sub>D<sub>6</sub>, δ, ppm): 7.68 (d, *J* = 7.5 Hz, 1H, C<sub>6</sub>H<sub>4</sub>), 7.44 (d, *J* = 8.4 Hz, 1H, C<sub>6</sub>H<sub>4</sub>), 7.00 (t, *J* = 7.2 Hz, 1H, C<sub>6</sub>H<sub>4</sub>), 7.17 (t, *J* = 7.4 Hz, 1H, C<sub>6</sub>H<sub>4</sub>), 6.76 (s, 4H, Mes), 2.18 (s, 12H, Me<sub>Mes</sub>), 2.17 (s, 6H, Me<sub>Mes</sub>), 1.63 (m, 2H), 1.39 (m, 2H), 1.23 (m, 2H), 1.15 (s, 6H, Me<sub>TMP</sub>), 1.00 (s, 6H, Me<sub>TMP</sub>).

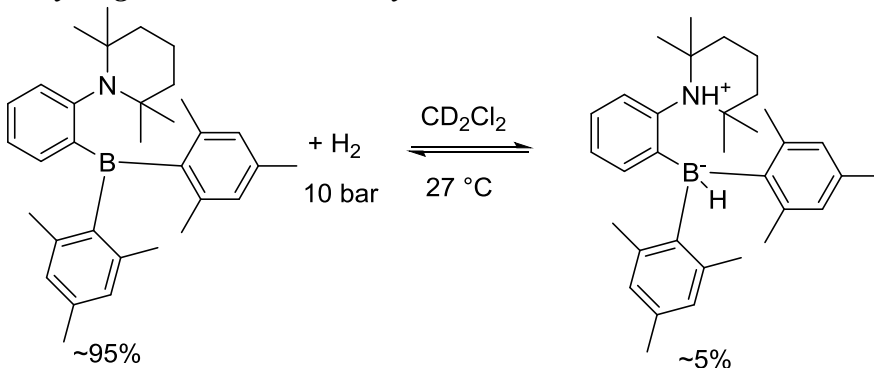
<sup>13</sup>C (75 MHz, C<sub>6</sub>D<sub>6</sub>, δ, ppm, B-C not observed): 155.05, 141.97, 138.94, 138.21, 133.20, 129.98, 129.54, 124.97, 56.01, 40.03, 34.06, 30.26, 25.04, 21.19, 18.82.

<sup>11</sup>B (160 MHz, C<sub>6</sub>D<sub>6</sub>, δ, ppm): 72.4 (s).





#### 6.4 Hydrogen addition to MesitylCAT

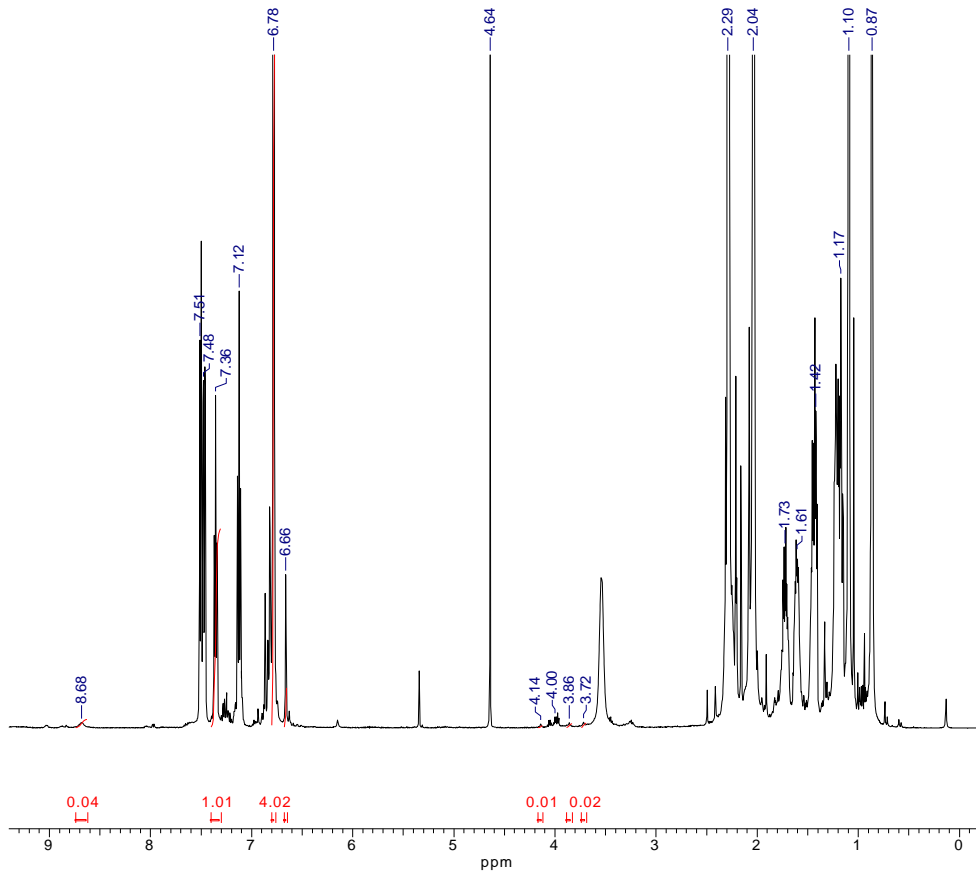


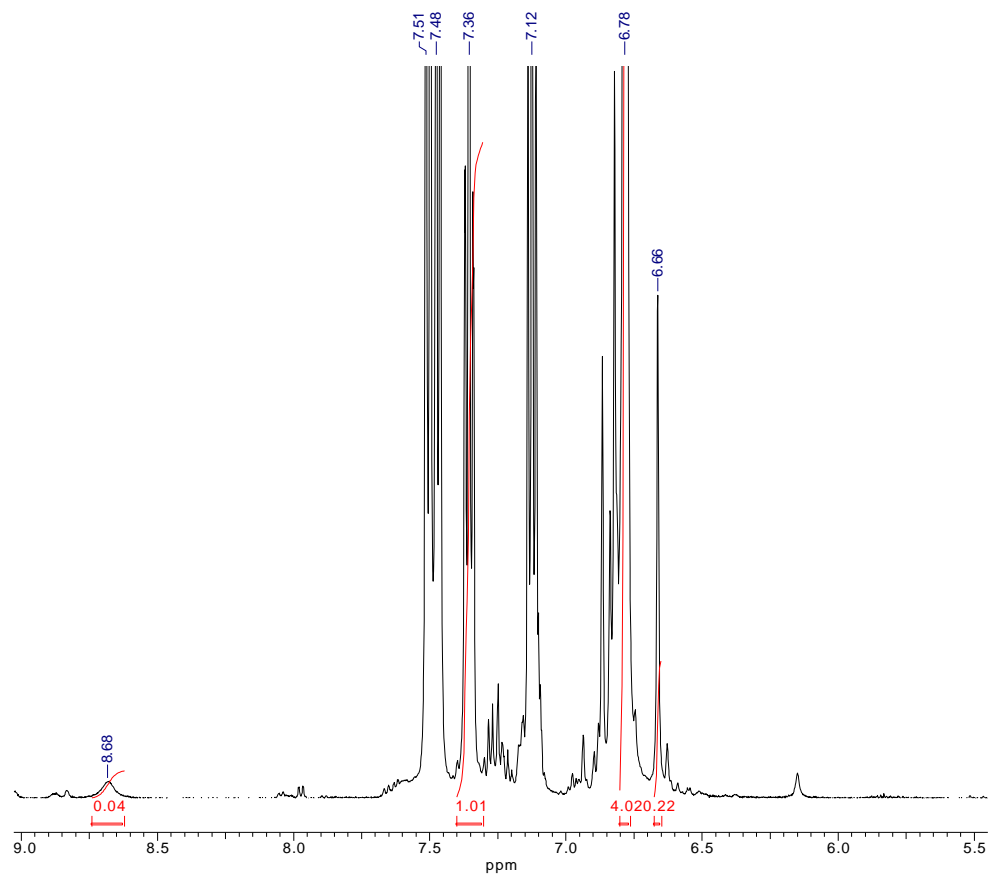
The NMR sample of 30 mg (0.065 mmol) of **2** in 0.3 ml of CD<sub>2</sub>Cl<sub>2</sub> under 10 bar H<sub>2</sub> was prepared as described for **PhenylCAT**. According to <sup>1</sup>H and <sup>11</sup>B NMR, the sample contained ~5 mol. % of the hydrogen adduct. Selected <sup>1</sup>H NMR signals attributed to the hydrogen adduct are provided below:

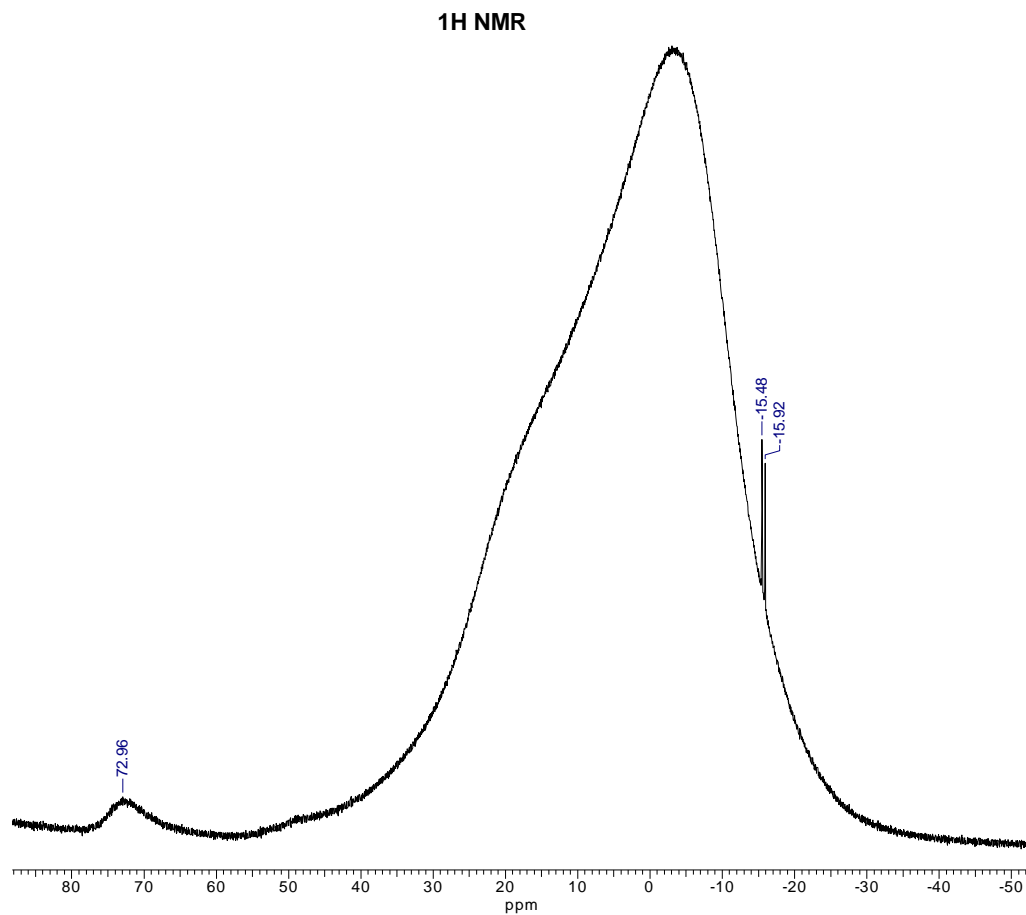
<sup>1</sup>H (500 MHz, C<sub>6</sub>D<sub>6</sub>, δ, ppm): 8.68 (s, 1H, NH), 6.66 (s, 4H, mesityl), 3.93 (q, *J* = 70.8 Hz, 1H, BH).

<sup>11</sup>B (160 MHz, C<sub>6</sub>D<sub>6</sub>, δ, ppm): 15.70 (d, *J*<sub>BH</sub> = 69.5 Hz)

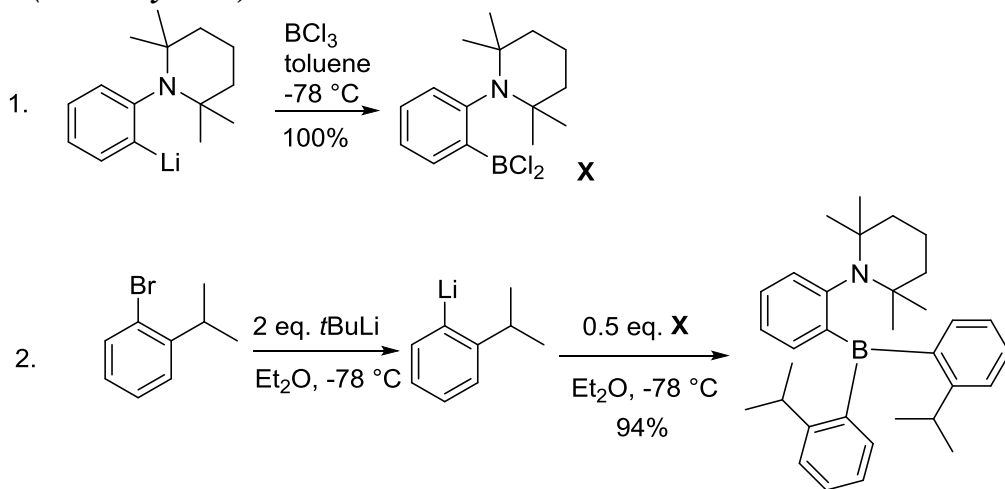
1H NMR







**6.5 1-(2-(Bis(2-isopropylphenyl)methyl)phenyl)-2,2,6,6-tetramethylpiperidine (iPrPhenylCAT)**



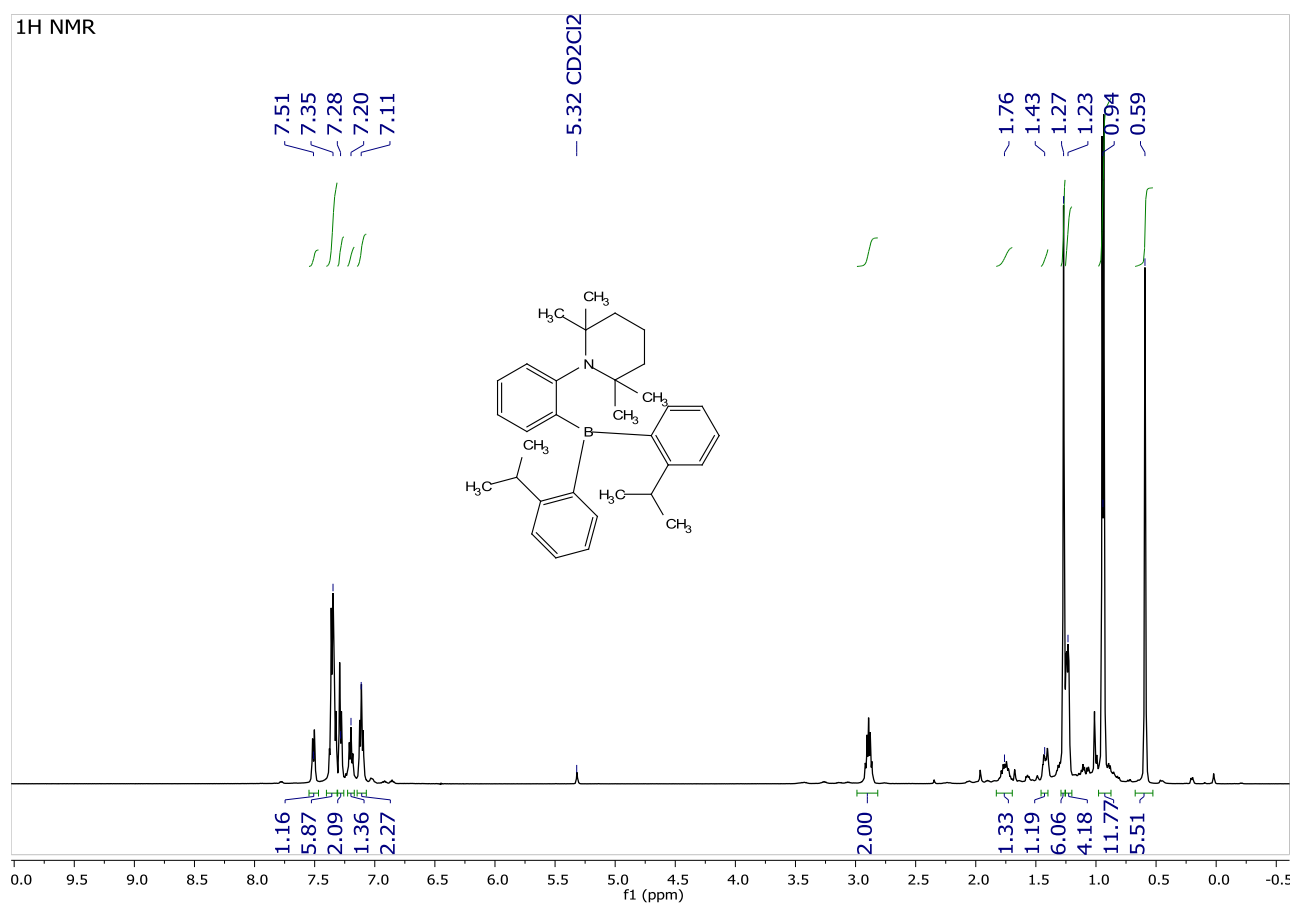
1. A solution of 282 mg of [2-(2,2,6,6-tetramethylpiperidin-1-yl)phenyl]lithium (1.25 mmol) in 4 ml of toluene was prepared in a 25 ml Schlenk tube and cooled to -90 °C. In another 25 ml Schlenk tube, a solution of BCl<sub>3</sub> (2.5 mmol, 2.5 ml of 1M solution in hexane) in 4 ml of toluene was prepared and cooled to -90 °C. The solution of the lithium compound was transferred in one portion via cannula to the Schlenk tube with a vigorously stirring solution of BCl<sub>3</sub>. The empty Schlenk tube that had contained the lithium compound was washed with additional 3 ml of toluene and the washing liquid was transferred to the reaction Schlenk tube as well. The reaction mixture immersed in a cooling bath was allowed to warm to room temperature naturally within 1 h and volatiles were stripped in vacuum. The residue was taken in 4 ml of hexane, filtered and washed additionally with 4 ml of hexane. Combined hexane extracts were evaporated to give 357 mg of the target compound **A** as yellow oil, which slowly solidified on standing into semi-solid crystalline material.

2. *tert*-Butyllithium (2.82 ml of 1.7 M solution in hexane, 4.8 mmol) was added dropwise to a solution of 0.477 g of 1-bromo-2-isopropylbenzene (2.4 mmol) in 6 ml of diethyl ether stirred at -78 °C. The mixture was stirred additionally for 15 min at -60 °C. Then the solution was cooled to -90°C, and the solution of 0.357 g of 1-(2-(dichloroboranyl)phenyl)-2,2,6,6-tetramethylpiperidine (**A**, 1.2 mmol) in 2.63 ml of hexane was added via syringe in one portion. The mixture was allowed to warm to room temperature and stirred overnight. The solvent was removed under reduce pressure; the residue was suspended in 10 ml of toluene and filtered. The filter cake was washed with additional portions (5x1 ml) of toluene and the filtrate was evaporated to dryness yielding 0.529 g (94.4%) of the target aminoborane as a slowly crystallizing upon standing yellow oil. The product was used without further purification.

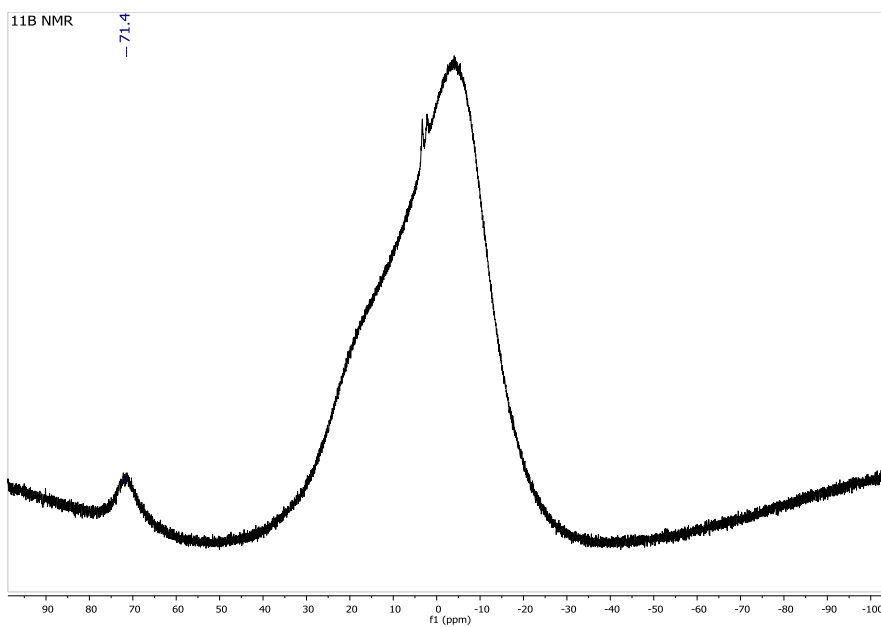
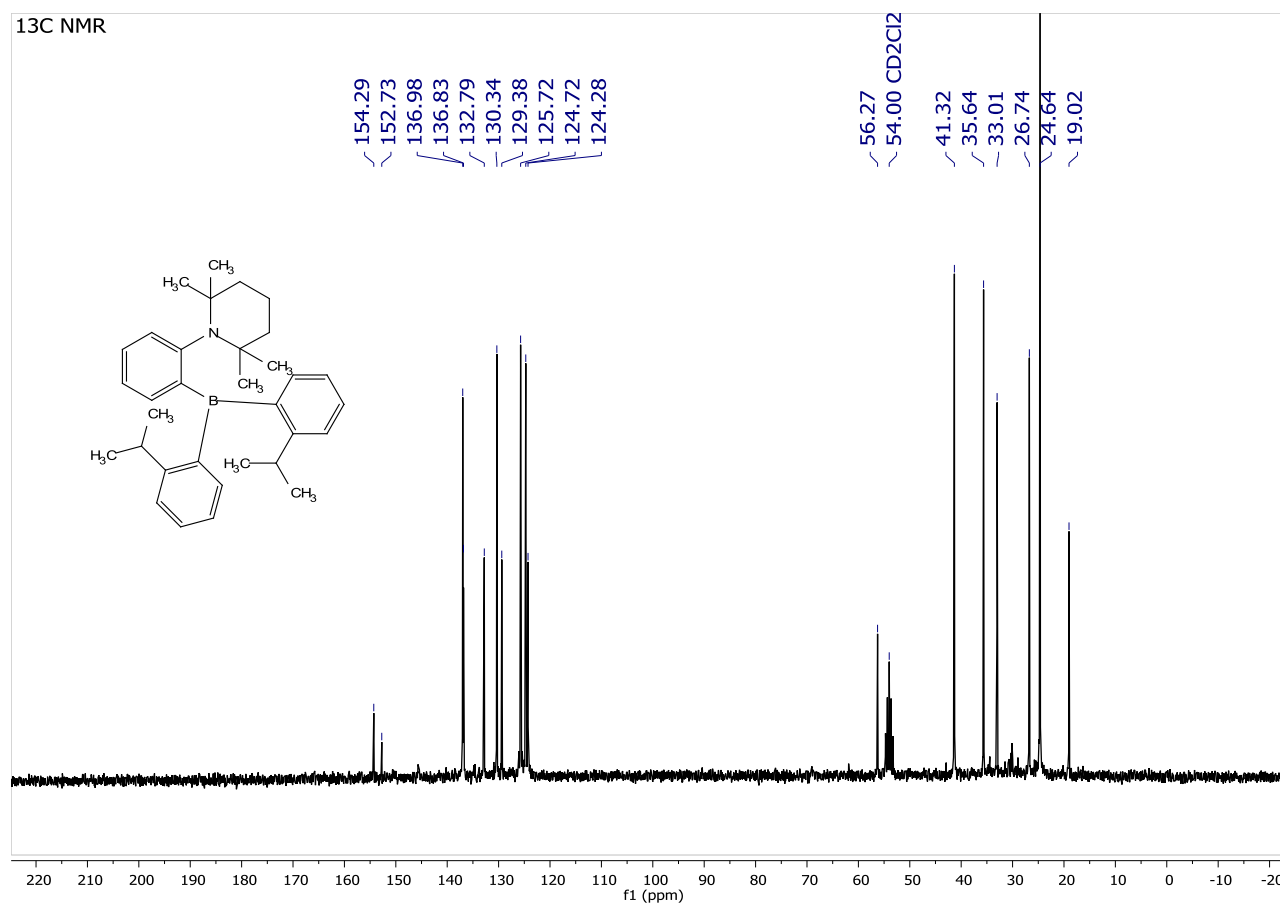
$^1\text{H}$  (500 MHz,  $\text{CD}_2\text{Cl}_2$ ,  $\delta$ , ppm): 7.51 (d,  $J = 7.8$  Hz, 1H), 7.35 (m 6H), 7.28 (m, 2H), 7.20 (t,  $J = 7.3$  Hz, 1H), 7.11 (t,  $J = 7.1$  Hz, 2H), 2.89 (hept,  $J = 6.8$  Hz, 2H,  $\text{CH}_{\text{iPr}}$ ), 1.76 (m, 1H,  $\text{CH}_2\text{CH}_2\text{CH}_2$ ), 1.43 (m, 1H,  $\text{CH}_2\text{CH}_2\text{CH}_2$ ), 1.27 (s, 6H,  $\text{Me}_{\text{TMP}}$ ), 1.23 (m, 4H,  $\text{CH}_2\text{CH}_2\text{CH}_2$ ), 0.94 (d,  $J = 6.8$  Hz, 12H,  $\text{Me}_{\text{iPr}}$ ), 0.59 (s, 6H,  $\text{Me}_{\text{TMP}}$ ).

$^{13}\text{C}$  NMR (75 MHz,  $\text{CD}_2\text{Cl}_2$ ,  $\delta$ , ppm, C-B not observed): 154.29, 152.73, 136.98, 136.83, 132.79, 130.34, 129.38, 125.72, 124.72, 124.28, 56.27, 41.32, 35.64, 33.01, 26.74, 24.64, 19.02.

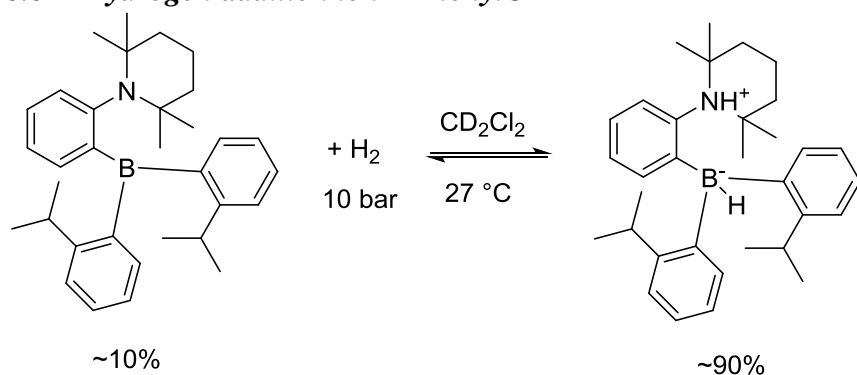
$^{11}\text{B}$  NMR (160 MHz,  $\text{CD}_2\text{Cl}_2$ ,  $\delta$ , ppm): 71.4 (br. s.).



13C NMR



## 6.6 Hydrogen addition to *iPrPhenylCAT*



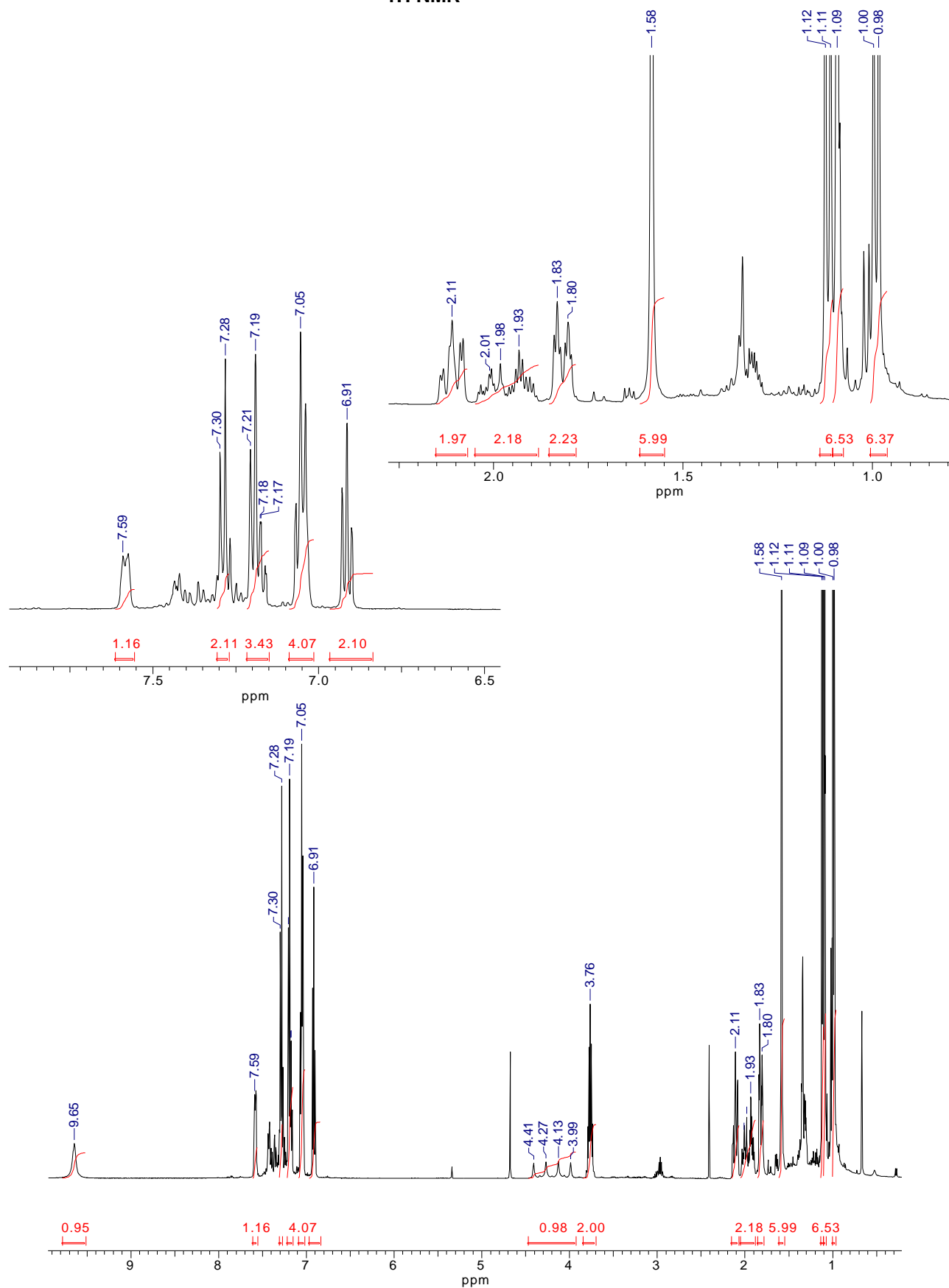
The NMR sample of 30 mg (0.064 mmol) of *iPrPhenylCAT* in 0.3 ml of  $\text{CD}_2\text{Cl}_2$  under 10 bar  $\text{H}_2$  was prepared as described for **PhenylCAT**.  $^1\text{H}$ ,  $^{13}\text{C}$ , and  $^{11}\text{B}$  NMR spectra were recorded and compared with the reference spectra which revealed an equilibrium of the starting *iPrPhenylCAT* and the respective  $\text{H}_2$  adduct in the  $\sim 10:90$  ratio.

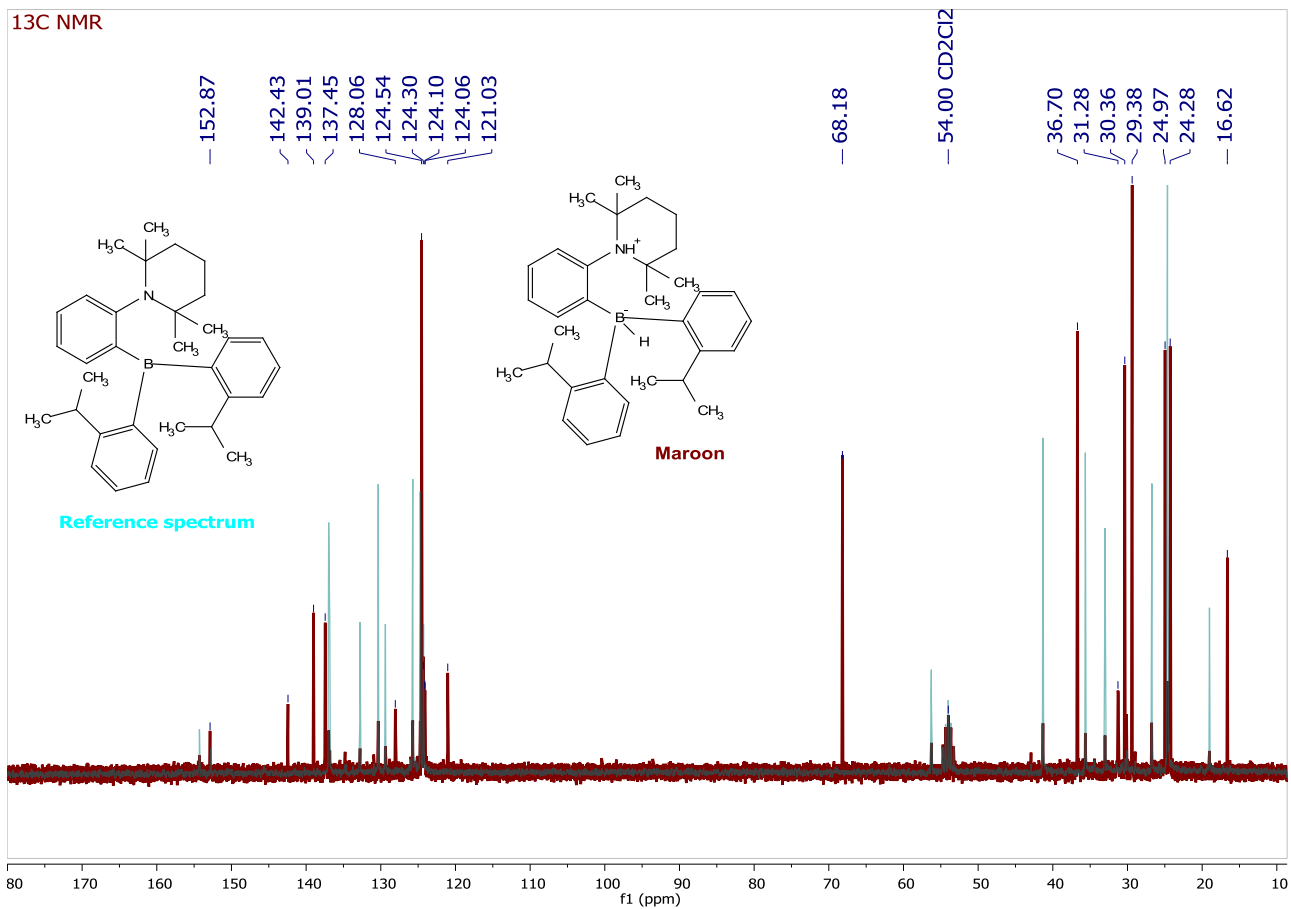
$^1\text{H}$  NMR (500 MHz  $\text{CD}_2\text{Cl}_2$ ,  $\delta$ , ppm): 9.65 (s, 1H, *NH*), 7.58 (m, 1H), 7.29 (d,  $J = 7.75$  Hz, 2H), 7.20 (d,  $J = 7.75$  Hz, 2H), 7.18 (m, 1H), 7.05 (m, 4H), 6.91 (td,  $J = 7.3, 1.3$  Hz, 1H), 4.20 (q,  $J = 70.3$  Hz, 1H, *BH*), 3.76 (hept,  $J = 7.0$  Hz, 1H), 2.11 (ddd,  $J = 14.5, 11.2, 4.1$  Hz, 2H), 2.01 (m, 1H), 1.93 (m, 1H), 1.82 (dt,  $J = 14.3, 3.9$  Hz, 2H), 1.58 (s, 6H,  $\text{Me}_{\text{TMP}}$ ), 1.12 (d,  $J = 6.9$  Hz, 6H,  $\text{Me}_{\text{iPr}}$ ), 1.09 (s, 6H,  $\text{Me}_{\text{TMP}}$ ), 0.99 (d,  $J = 6.8$ , 6H,  $\text{Me}_{\text{iPr}}$ ).

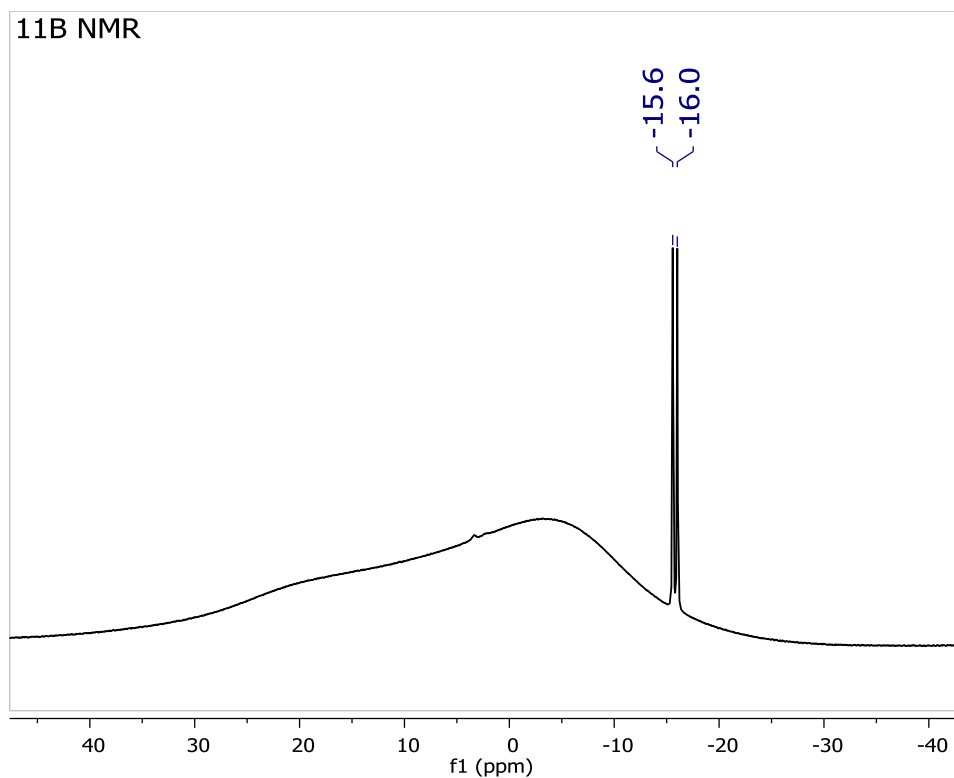
$^{13}\text{C}$  NMR (75 MHz,  $\text{CD}_2\text{Cl}_2$ ,  $\delta$ , ppm, C-B not observed): 152.87, 142.43, 139.01, 137.45, 128.06, 124.54, 124.30, 124.10, 124.06, 121.03, 68.18, 36.70, 31.28, 30.36, 29.38, 24.97, 24.28, 16.62.

$^{11}\text{B}$  NMR (160 MHz,  $\text{CD}_2\text{Cl}_2$ ,  $\delta$ , ppm): -15.8 (d,  $J = 70.1$  Hz).

# 1H NMR







## 7 Computational results

Potential energy surface scan calculation was carried out to explore the rotation of the  $\text{BH}_3$  moiety in BorylCAT- $\text{H}_2$ . The  $\text{C}_\text{N}\text{C}_\text{B}\text{BH}$  dihedral was scanned between  $0^\circ$  and  $180^\circ$  by  $10^\circ$  increments (see Figure S10). Due to the symmetry of  $\text{BH}_3$  group, the potential energy curve is periodic in  $120^\circ$ . The maximum value is 3.8 kcal/mol at  $60^\circ$ . Using this structure, the transition state of the rotation was identified.

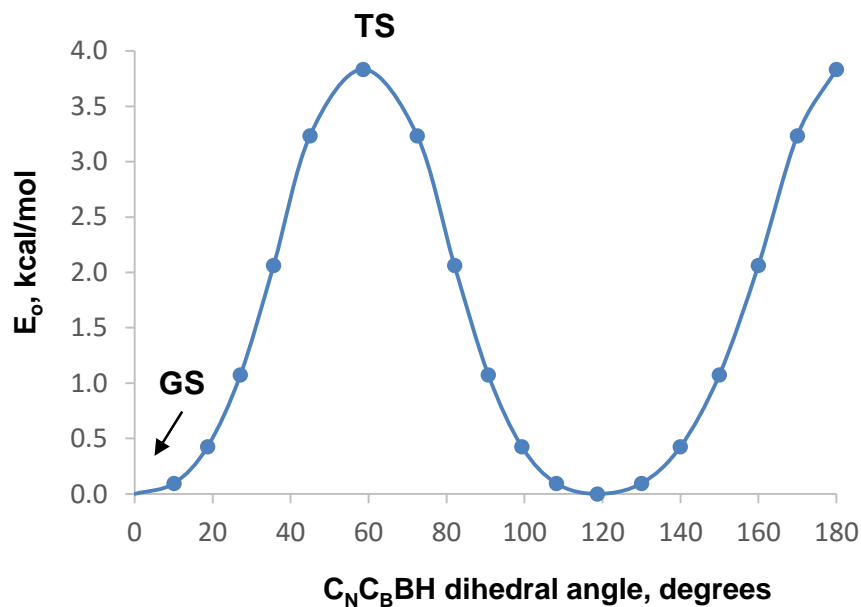


**Figure S10.** Potential energy surface scan of rotation of BH<sub>3</sub> moiety in BorylCAT-H<sub>2</sub>.

The optimized structures of BorylCAT-H<sub>2</sub> and the BH<sub>3</sub> rotation TS are shown on Figure S11. In the ground state, one of the BH<sub>3</sub> hydrogens is in the plane of the phenyl ring and points toward the NH proton. The distance between the NH and BH hydrogens is 1.44 Å. In the TS, the BH<sub>3</sub> moiety is rotated by 60°. Two of the BH hydrogens are equivalent and they 2.00 Å from the NH hydrogen.

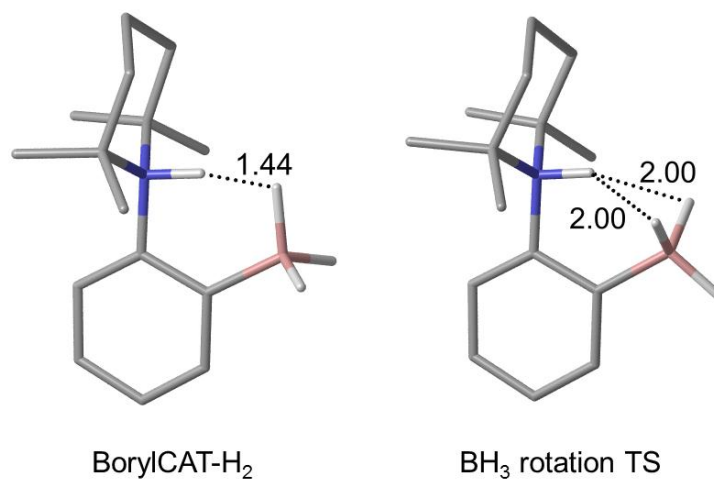


**Figure S11.** Optimized structures of BorylCAT-H<sub>2</sub> and the BH<sub>3</sub> rotational TS, respectively. Dihydrogen bond distances are shown in Ångstroms.

The variation of calculated  $J_{\text{NHBB}}$  coupling constant with respect to the  $\text{C}_\text{N}\text{C}_\text{B}\text{BH}$  dihedral angle between 0 and 180° is shown on Figure S12. The coupling constant has the highest value (6.2 Hz) in the ground state (corresponding to 0°), where the  $\text{NH}\cdots\text{HB}$  distance is the shortest. The TS corresponds to 60° with  $J_{\text{NHBB}} = -1.4$  Hz. The coupling constant that should be related to the experimentally observed value is the weighted average of  $J_{\text{NHBB}}$  data obtained several conformations. Boltzmann factors computed from the potential energy curve of  $\text{BH}_3$  rotation were used for the averaging, which resulted in  $J_{\text{NHBB}} = 2.1$  Hz.

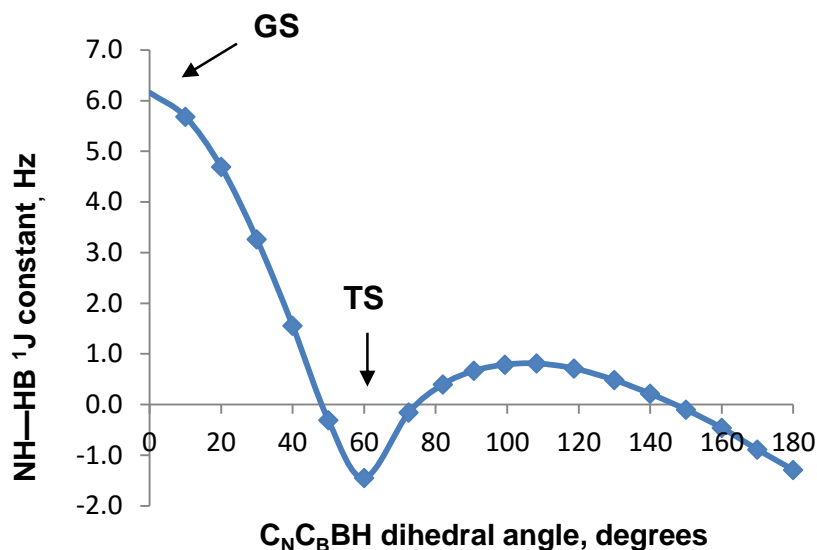


**Figure S12.** Calculated  $J_{\text{NHBB}}$  coupling constants for conformers of BorylCAT- $\text{H}_2$  with  $\text{C}_\text{N}\text{C}_\text{B}\text{BH}$  values ranging from 0 to 180°.

### 7.1 Cartesian coordinates of BorylCAT- $\text{H}_2$ and the $\text{BH}_3$ rotation TS

Cartesian coordinates of  $\omega\text{B97XD}/6\text{-}311\text{G(d,p)}$  optimized geometries are given below in standard XYZ format (units are in Å). First line indicates total number of atoms, second line is molecule name.

```

43
BorylCAT-H2
C  0.000000  0.000000  0.000000
C -0.000000  0.000000  1.392711

```

C	-1.158668	0.000100	2.174342
C	-2.361149	0.000154	1.449527
C	-2.396833	0.000129	0.065084
C	-1.212734	0.000066	-0.668911
N	1.253871	-0.000029	2.174041
C	2.029591	-1.331309	2.176553
C	3.046137	-1.245309	3.324994
C	3.922446	-0.000015	3.279438
C	3.046124	1.245270	3.324956
C	2.029596	1.331215	2.176497
C	1.017119	-2.438645	2.489221
C	2.712707	-1.656937	0.849881
C	1.017092	2.438535	2.489094
C	2.712692	1.656756	0.849799
B	-1.173282	0.000154	3.798430
H	-1.727832	1.006916	4.202473
H	-1.728321	-1.006302	4.202564
H	3.653848	2.153618	3.299120
H	2.496157	1.259727	4.273285
H	2.496188	-1.259748	4.273334
H	3.653870	-2.153651	3.299170
H	4.553768	-0.000023	2.385016
H	4.602452	-0.000002	4.134792
H	0.426211	-2.209831	3.378326
H	0.330239	-2.600100	1.657585
H	1.569763	-3.364330	2.666884
H	3.157012	-2.650319	0.947855
H	1.995809	-1.704408	0.031217
H	3.511802	-0.968538	0.583333
H	0.330180	2.599887	1.657464
H	0.426218	2.209756	3.378231
H	1.569703	3.364257	2.666669
H	3.157140	2.650076	0.947741
H	3.511672	0.968241	0.583207
H	1.995751	1.704313	0.031174
H	0.921492	-0.000028	-0.565973
H	-1.232957	0.000072	-1.752463
H	-3.350342	0.000174	-0.452445
H	-3.291772	0.000203	2.007718
H	0.823008	0.000014	3.139078
H	-0.026928	-0.000109	4.301866

43

BH<sub>3</sub> rotation TS of BorlyCAT-H<sub>2</sub>

C	-1.619936	-0.000450	-1.383752
C	-1.099588	-0.000168	-0.095970
C	-1.874772	0.000189	1.069983
C	-3.259607	0.000221	0.851517

C	-3.815775	-0.000074	-0.420327
C	-2.998021	-0.000419	-1.545106
N	0.360197	-0.000029	0.157595
C	1.101833	-1.325562	-0.150978
C	2.398786	-1.259096	0.669380
C	3.224280	0.000290	0.416304
C	2.398553	1.259601	0.669007
C	1.101551	1.325592	-0.151315
C	0.231345	-2.482695	0.346792
C	1.382332	-1.561770	-1.635566
C	0.230852	2.482670	0.346235
C	1.381891	1.561501	-1.635984
B	-1.221538	0.000183	2.563420
H	-0.498971	-0.984199	2.717110
H	-0.497718	0.983704	2.716856
H	2.984407	2.154930	0.444136
H	2.132203	1.313846	1.731433
H	2.132413	-1.313067	1.731815
H	2.984817	-2.154384	0.444806
H	3.620277	0.000174	-0.604159
H	4.093615	0.000472	1.078200
H	-0.101038	-2.329782	1.372667
H	-0.646831	-2.618992	-0.285976
H	0.831987	-3.394485	0.304623
H	1.692078	-2.604005	-1.738503
H	0.488329	-1.433830	-2.244499
H	2.180991	-0.948353	-2.042866
H	-0.647400	2.618620	-0.286500
H	-0.101407	2.329975	1.372182
H	0.831304	3.394572	0.303778
H	1.691350	2.603790	-1.739225
H	2.180679	0.948184	-2.043181
H	0.487871	1.433154	-2.244811
H	-0.983007	-0.000691	-2.257602
H	-3.425114	-0.000650	-2.541129
H	-4.894120	-0.000040	-0.539516
H	-3.909750	0.000488	1.719665
H	0.342351	0.000143	1.195746
H	-2.085353	0.000734	3.413372

## 8 REFERENCES

S1. A. D. Bain, B. Berno, *Prog. Nucl. Magn. Reson. Spectrosc.*, 2011, **59**, 223-244.

S2. K. Chernichenko, M. Nieger, M. Leskelä, T. Repo, *Dalton Trans.*, 2012, **41**,

9029-9032.